


## Quantum annealing with error mitigation

Yuta Shingu<sup>1,2,\*</sup>, Tetsuro Nikuni<sup>1,†</sup>, Shiro Kawabata<sup>2,3,‡</sup> and Yuichiro Matsuzaki<sup>2,3,§</sup>

<sup>1</sup>*Department of Physics, Graduate School of Science, Tokyo University of Science, Shinjuku, Tokyo 162-8601, Japan*

<sup>2</sup>*Global Research and Development Center for Business by Quantum-AI Technology (G-QuAT), National Institute of Advanced Industrial Science and Technology (AIST), 1-1-1 Umezono, Tsukuba, Ibaraki 305-8568, Japan*

<sup>3</sup>*NEC-AIST Quantum Technology Cooperative Research Laboratory, National Institute of Advanced Industrial Science and Technology (AIST), 1-1-1 Umezono, Tsukuba, Ibaraki 305-8568, Japan*

 (Received 21 November 2022; revised 13 June 2023; accepted 12 February 2024; published 2 April 2024)

Quantum annealing (QA) is one of the methods to prepare a ground state of a problem Hamiltonian. In the absence of noise, QA can accurately estimate the ground-state energy if the adiabatic condition is satisfied. However, in practice, systems are known to suffer from decoherence. Meanwhile, considerable research effort has been devoted to noisy intermediate-scale quantum (NISQ) computation. For practical NISQ computation, many error-mitigation (EM) methods have been proposed to mitigate the effects of noise. This paper proposes a QA strategy combined with an EM method, namely, dual-state purification, to suppress the effects of decoherence. Our protocol consists of four parts: the conventional dynamics, single-qubit projective measurements, the Hamiltonian dynamics corresponding to an inverse map of the first dynamics, and postprocessing of the measurement results. Importantly, our protocol works without two-qubit gates that require pulse operations; hence, it is suitable for devices designed for practical QA. In addition, we present numerical calculations to show that our protocol is more accurate than the conventional QA in estimating the ground-state energy under decoherence.

DOI: [10.1103/PhysRevA.109.042606](https://doi.org/10.1103/PhysRevA.109.042606)

### I. INTRODUCTION

Quantum annealing (QA) [1–5] is a promising approach for obtaining the ground state of a problem Hamiltonian  $H_P$ . Initially, the system is prepared as the ground state of a driver Hamiltonian  $H_D$ . In QA, we employ a time-dependent total Hamiltonian that changes from  $H_D$  to  $H_P$ , and we let the state evolve by such a Hamiltonian. As long as the adiabatic condition is satisfied, we can obtain the ground state of  $H_P$  after the dynamics without noise [6–10].

Specifically, we can obtain the ground state of the Ising-type problem Hamiltonian by measuring the state after QA in the computational basis, as long as the state has a finite population of the ground state [11–13]. The density matrix after QA can be expanded in the energy eigenbasis as follows:  $\rho = \sum_{j,j'} d_{j,j'} |E_j\rangle \langle E_{j'}|$  where  $d_{j,j'}$  denotes a coefficient,  $p_j \equiv d_{j,j}$  denotes a population, and  $|E_j\rangle$  denotes an eigenvector of the problem Hamiltonian. In this case, the probability of obtaining the ground state with the measurement in the computational basis is expressed as  $1 - (1 - p_0)^{N_{\text{trial}}}$  [14], where  $p_0$  denotes the population of the ground state and  $N_{\text{trial}}$  denotes the number of trials. Thus, we can obtain the ground state after multiple trials as long as  $p_0$  has a nonzero value.

If the problem Hamiltonian is diagonal in the computational basis, we can represent the ground state on a computational basis. This means that, although we could not find the ground state efficiently, we can represent it with classical computation. On the other hand, if the problem Hamiltonian contains nondiagonal elements, the ground state is typically an entangled state and difficult to simulate with a classical computer. If one can implement fault-tolerant quantum computation, the phase estimation algorithm is an effective way to estimate the energy of  $H_P$  [15–17]. On the other hand, in the NISQ era, QA is a candidate to prepare and explore the properties of such entangled states, which can be used for quantum simulation and quantum chemistry [18,19]. In this case, the main objective is to estimate the energy of the ground state, which is the focus of our study. For such a Hamiltonian, we cannot obtain the ground state of the problem Hamiltonian by the measurements in the computational basis after QA. The expectation value of the problem Hamiltonian with the density matrix  $\rho$  after QA is expressed as  $\langle H_P \rangle = \text{Tr}[H_P \rho] = \sum_j p_j E_j$ . The problem Hamiltonian  $H_P$  can be expanded by the products of the Pauli matrices such as  $H_P = \sum_i c_i \sigma_i$ , where  $c_i$  denotes a coefficient and  $\sigma_i$  denotes a tensor product of the Pauli matrices, which we refer to as Pauli product. To obtain the expectation value of the problem Hamiltonian, one must determine the expectation value of each term by the measurements in the Pauli basis after QA, and take the summation of these expectation values. Notably, a finite population of the excited state after QA leads to an error in the estimation of the ground-state energy. Therefore, we must prepare the ground state with high fidelity to accurately estimate the ground-state energy.

\* [1222705@ed.tus.ac.jp](mailto:1222705@ed.tus.ac.jp)

† [nikuni@rs.tus.ac.jp](mailto:nikuni@rs.tus.ac.jp)

‡ [s-kawabata@aist.go.jp](mailto:s-kawabata@aist.go.jp)

§ [ymatsuzaki872@g.chuo-u.ac.jp](mailto:ymatsuzaki872@g.chuo-u.ac.jp)

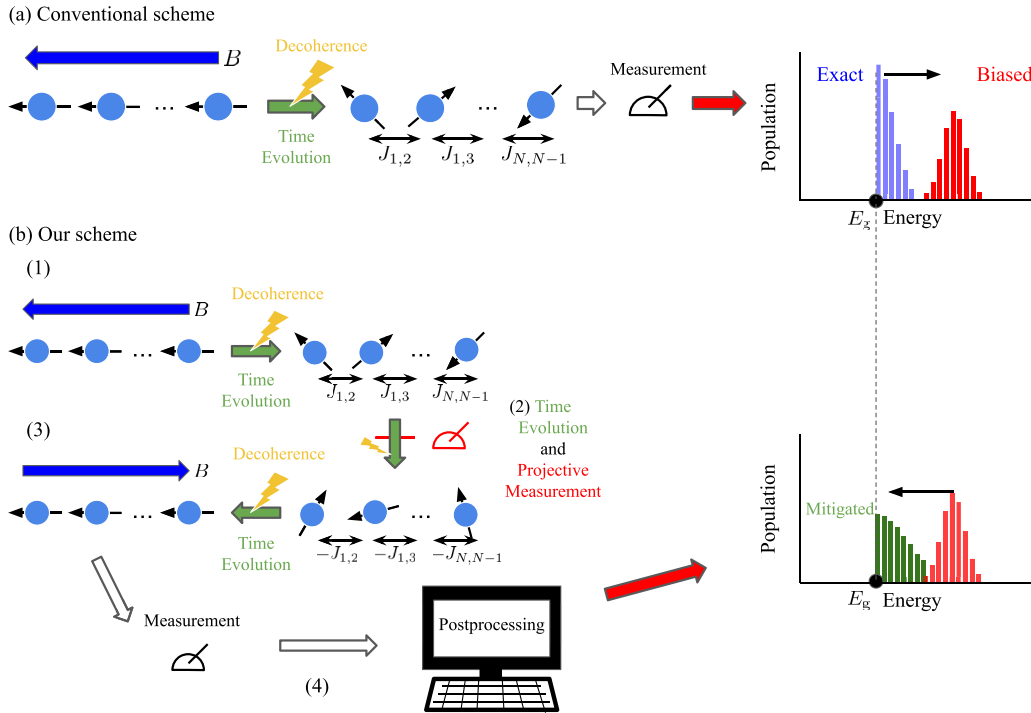


FIG. 1. Conceptual diagram showing the difference between the conventional QA scheme and our QA scheme. (a) In the conventional scheme, one gradually changes the total Hamiltonian from a driver Hamiltonian  $H_D$  to a problem Hamiltonian  $H_P$ . The blue bars in the graph denote the exact populations without decoherence, which can include the effects of nonadiabatic transitions. By decoherence, we actually obtain the biased populations as indicated by the red bars. In this case, the estimation of the ground-state energy  $E_g$  of  $H_P$  will be inaccurate if there is decoherence. (b) Our scheme, which incorporates the EM method, consists of four parts: (1) the conventional dynamics, (2) switching the sign of the coefficients in  $H_P$  and single-qubit projective measurements, (3) the Hamiltonian dynamics corresponding to an inverse map of the first dynamics, and (4) postprocessing of the measurement results. The green bars denote the populations in which the noise effects are mitigated. Owing to the EM method, we can estimate the ground-state energy more accurately than the conventional QA shown in (a).

However, QA suffers from nonadiabatic transitions and decoherence [20–28]. There are two types of decoherence called thermal excitation and dephasing, characterized by  $T_1$  and  $T_2$ , respectively. Especially in QA, thermal excitation is problematic because this induces unwanted transitions from the ground to the excited states. If the dynamics are not sufficiently slow to satisfy the adiabatic condition, unwanted transitions occur from the ground state to excited states. Meanwhile, if the timescale of QA is comparable with or longer than the thermal excitation time of the qubit, the system will be affected by decoherence, which also induces unwanted transitions to the excited states. Thus, the estimation of the ground-state energy will be biased, as shown in Fig. 1(a).

Many theoretical and experimental studies have been conducted to realize practical noisy intermediate-scale quantum (NISQ) computation [29–31]. We can employ NISQ devices to perform quantum computation using tens to thousands of qubits, with gate errors of  $10^{-3}$  or lower [32,33]. Here, the gate error for a quantum computer means the probability when the corresponding quantum gate operation fails. Many algorithms for NISQ computation have been proposed. Typically, variational quantum circuits are used to generate a trial wave function in order to minimize the cost function [34–38]. In these algorithms, one must measure observables on the qubits corresponding to the trial wave function. In the actual devices, noise prevents one from obtaining the accurate

expectation values of the observables, thereby degrading the algorithm performance. Sophisticated techniques referred to as “error mitigation” (EM) suppress the effects of noise by implementing additional quantum gates and postprocessing with classical computation [30,35,39–64].

Particularly, the virtual distillation (VD) method, which is known as the exponential error suppression (EES) method, can mitigate the error without knowing the details of the noise model [65–68]. Suppose that  $N$  qubits are required to implement a quantum algorithm without EM. In VD (EES), one must prepare  $M$  copies of noisy quantum states  $\rho$  composed of  $N$  qubits to mitigate the error. We assume that these states are generated by the same quantum circuit and influenced by the same noise model. By entangling gates between  $M$  copies of a quantum state  $\rho$ , one can obtain  $\langle O \rangle_{\text{VD}}^{(M)} = \text{Tr}[O \rho_{\text{VD}}^{(M)}]$  with  $\rho_{\text{VD}}^{(M)} = \rho^M / \text{Tr}[\rho^M]$ . The advantage of this scheme is that the population of the dominant eigenvector of  $\rho$  approaches unity; hence, the stochastic errors are exponentially suppressed as one increases  $M$ . However, VD (EES) requires  $MN$  qubits of the quantum state, which involves high costs for NISQ computers.

Recently, an alternative scheme called “dual-state purification” was proposed to overcome the aforementioned problem [69]. Let us consider the specific case  $M = 2$ . In this scheme, one can effectively prepare two copies of the quantum state on the same qubits. One can physically generate one of them in an original quantum circuit, and the other one can be

virtually prepared using the inverse of the original circuit, which is designed as the conjugate transpose of the original circuit when there is no error. By decomposing an observable  $O$  into Pauli products  $\{\sigma_i\}$ , one obtains the expectation value  $\langle O \rangle$  as  $\sum_i a_i \langle \sigma_i \rangle$ , where  $a_i$  is a coefficient. In dual-state purification, one calculates each expectation value  $\langle \sigma_i \rangle$  with each corresponding circuit and then takes the summation to compute the expectation value  $\langle O \rangle$ . The entire circuit for dual-state purification consists of the original circuit, the projective measurement of a Pauli product  $\sigma_i$ , the inverse circuit, and the projective measurement to the initial state. After postprocessing operations with classical computation, one obtains the expectation value of  $O$ , where the stochastic errors during the implementation of the quantum circuits are mitigated. Importantly, this scheme requires only  $N$  qubits.

In this paper, we propose QA with dual-state purification. As shown in Fig. 1(b), (1) we perform the same dynamics as the conventional QA, (2) we change the sign of the problem Hamiltonian as fast as possible within the limitations of the devices, and perform single-qubit projective measurements, (3) we gradually decrease (increase) the driver (problem) Hamiltonian, and (4) we postprocess the measurement results. Our strategy requires a quantum device that can not only create the dynamics described by the QA Hamiltonian but also perform arbitrary single-qubit operations. Moreover, we numerically demonstrate that our strategy provides a more accurate estimation than that provided by the conventional QA.

## II. QUANTUM ANNEALING

Here, we review the conventional QA to obtain the ground state and the ground-state energy of a problem Hamiltonian  $H_P$  [1–3]. Throughout this paper, we set  $\hbar = 1$ . We choose a uniform transverse field on the spins as a driver Hamiltonian (i.e.,  $H_D = -B \sum_{i=1}^N \hat{\sigma}_i^x$ ,  $B > 0$ ), where  $N$  denotes the number of qubits and  $B$  denotes a coefficient. Furthermore, the system is initially prepared as  $|+\rangle^{\otimes N}$ , which is the ground state of the driver Hamiltonian  $H_D$ , where  $|+\rangle = \frac{1}{\sqrt{2}}(|0\rangle + |1\rangle)$  denotes the eigenstate of  $\hat{\sigma}^x$  and  $|0\rangle$  ( $|1\rangle$ ) denotes the eigenstate of  $\hat{\sigma}^z$  which has the eigenvalue  $+1$  ( $-1$ ). We change the total Hamiltonian  $H_{\text{CQA}}(t)$  from the driver Hamiltonian  $H_D$  to the problem Hamiltonian  $H_P$  over time as follows:

$$H_{\text{CQA}}(t) = A_{\text{CQA}}(t)H_D + B_{\text{CQA}}(t)H_P, \quad (1)$$

where  $A_{\text{CQA}}(t)$  and  $B_{\text{CQA}}(t)$  are time-dependent coefficients. The coefficients of the total Hamiltonian in QA are here given by

$$A_{\text{CQA}}(t) = 1 - \frac{t}{T} \quad (t : 0 \rightarrow T),$$

$$B_{\text{CQA}}(t) = \frac{t}{T} \quad (t : 0 \rightarrow T),$$

where  $T$  is the annealing time. If the total Hamiltonian  $H_{\text{CQA}}(t)$  is varied sufficiently slowly and the energy level crossing does not occur, the adiabatic theorem guarantees that the ground state of  $H_P$  can be obtained.

The estimation of the ground-state energy by QA involves two main problems: environmental decoherence and nonadiabatic transitions [20–28]. By performing QA with a longer

time schedule, we can avoid the effects of nonadiabatic transitions. However, a longer time schedule will make the quantum states more prone to decoherence. This tradeoff relationship makes it difficult to solve practical problems with QA.

Many studies have investigated the suppression of nonadiabatic transitions and decoherence during QA. An inhomogeneous driver Hamiltonian can be used to accelerate QA for a specific problem Hamiltonian [70,71]. Seki *et al.* showed that the performance of QA for certain types of problem Hamiltonians can be improved with “nonstoquastic” Hamiltonians that have negative off-diagonal matrix elements [72,73]. The energy gap between the ground state and the first excited state can be estimated in a robust manner against nonadiabatic transitions [74–76]. The specific choice of the driver Hamiltonian to preserve the symmetry of the system is known to be useful for efficient QA [77,78]. It is known that shortcuts to adiabaticity and counterdiabatic driving can avoid nonadiabatic transitions [18,79–94]. Moreover, several studies have investigated the suppression of environmental noise. Error correction with ancillary qubits can be adopted to suppress decoherence during QA [95]. A scheme with a decoherence-free subspace for QA has also been proposed [96]. Spin-lock techniques are beneficial for applying long-lived qubits to QA [97–99]. In addition, there are several schemes for improving the performance of QA by using nonadiabatic transitions and quenching [100–107] and degenerating two-level systems [108]. Variational methods have also been applied to QA in order to suppress nonadiabatic transitions and decoherence [85,109–111].

## III. DUAL-STATE PURIFICATION

In this section, we review an EM method called dual-state purification [69]. First, we introduce VD (EES) methods for NISQ devices that dual-state purification is based on. In the VD (EES) methods [65–67,112], by using two copies of a noisy state  $\rho$ , we can obtain a purified state  $\rho_{\text{VD(EES)}}^{(2)} = \rho^2 / \text{Tr}[\rho^2]$ . Let us assume that the noisy state  $\rho$  is expressed by an orthogonal basis  $\{|\psi_n\rangle\}_{n=0}^{2^N-1}$  as

$$\rho = (1-p)|\psi_0\rangle\langle\psi_0| + p \sum_{n=1}^{2^N-1} \lambda_n |\psi_n\rangle\langle\psi_n|, \quad (2)$$

where  $p$  denotes an error probability,  $\lambda_n \geq 0$ , and  $\sum_{n=1}^{2^N-1} \lambda_n = 1$ . Let us call  $|\psi_0\rangle$  a dominant state, and we define  $\rho_e = \sum_{n=1}^{2^N-1} \lambda_n |\psi_n\rangle\langle\psi_n|$ . In this case, the purified state  $\rho_{\text{VD(EES)}}^{(2)}$  is closer to the dominant state than the original state for  $p > \frac{1}{2}$ . The expectation value of an observable  $O$  is estimated as  $\langle O \rangle = \langle \psi_0 | O | \psi_0 \rangle \simeq \text{Tr}[O\rho^2] / \text{Tr}[\rho^2]$ . Furthermore, the noisy state can also be expressed in another form as

$$\rho = \eta |\phi_{\text{id}}\rangle\langle\phi_{\text{id}}| + (1-\eta) \sum_{k=1}^d \mu_k |\chi_k\rangle\langle\chi_k|, \quad (3)$$

where  $|\phi_{\text{id}}\rangle = U|\vec{0}\rangle$  denotes the ideal state,  $U$  denotes a unitary operator without any noise,  $|\vec{0}\rangle$  denotes an initial state. Here,  $\eta \geq 0$  and  $\sum_{k=1}^d \mu_k = 1$  are satisfied. Note that the overlap  $\langle \phi_{\text{id}} | \chi_k \rangle$  is not always 0. Although the dominant state is not necessarily equal to the ideal state because of a small

coherent mismatch in practical cases,  $\langle \psi_0 | O | \psi_0 \rangle$  is known to be a good approximation to  $\langle \phi_{\text{id}} | O | \phi_{\text{id}} \rangle$  [65,66,112]. On the other hand, if there are only incoherent errors,  $|\phi_{\text{id}}\rangle = |\psi_0\rangle$  is satisfied. However, in this scheme, the required number of qubits is twice as large as that of the original scheme without VD (EES) methods.

Another EM scheme called dual-state purification can be implemented with the same number of qubits as the original scheme [69]. Here, we consider a situation where there is only incoherent error (i.e., the dominant state is equal to the ideal state). To discuss dual-state purification, we consider a noisy map  $\mathcal{F}(\bullet) = \sum_k F_k \bullet F_k^\dagger$ , where  $\{F_i\}$  denote Kraus operators and  $\bullet$  denotes an arbitrary matrix. When the noise amplitude is significantly small, this map is close to the ideal unitary operator  $U$  [i.e.,  $\mathcal{F}(\bullet) \simeq U \bullet U^\dagger$ ]. Since any unitary operation  $U$  is constructed with the dynamics of the corresponding Hamiltonian, we can always prepare the inverse dynamics  $U^\dagger$  by switching all the signs of coefficients of the Hamiltonian. We consider the case where, due to noise, we cannot realize the ideal  $U^\dagger$  and the actual dynamics is described by  $\mathcal{G}(\bullet) = \sum_k G_k \bullet G_k^\dagger$ , where  $\{G_i\}$  denote Kraus operators. If the noise effect can be ignored, this noisy map  $\mathcal{G}(\bullet)$  can be approximated as  $U^\dagger \bullet U$ .

By using the operations  $\mathcal{F}$  and  $\mathcal{G}$ , we obtain

$$\langle \vec{0} | \mathcal{G}(\mathcal{F}(|\vec{0}\rangle\langle\vec{0}|)) | \vec{0} \rangle = \text{Tr}[\bar{\rho}] = \text{Tr}[\bar{\rho}\rho], \quad (4)$$

where  $\rho = \mathcal{F}(|\vec{0}\rangle\langle\vec{0}|)$ ,  $\bar{\rho} = \mathcal{G}(\rho)$ , and  $\bar{\rho} = \mathcal{G}(|\vec{0}\rangle\langle\vec{0}|)$ . We refer to  $\bar{\rho}$  as the dual map of  $\rho$ , and we refer to  $\bar{\rho}$  as the dual state. Although we call this a dual state, this may not be a density matrix because the dual map may not be a completely positive trace-preserving (CPTP) map. However, this is called a dual state in the original paper [69], and thus we adopt the same terminology as the previous study. When the noise strength is low enough, we can approximate  $\bar{\rho}(\bullet)$  as  $U \bullet U^\dagger$  and  $\text{Tr}[\bar{\rho}\rho]$  as  $\text{Tr}[\rho^2]$ .

Next, we show how dual-state purification increases the population of the ideal state  $|\phi_{\text{id}}\rangle$ . Here, we assume that  $\bar{\rho} = (1 - \bar{p})|\phi_{\text{id}}\rangle\langle\phi_{\text{id}}| + \bar{p}\bar{\rho}_e$ , where  $\bar{\rho}_e$  denotes a normalized positive-semidefinite state and  $\bar{p}$  denotes an error probability to satisfy  $1 - \bar{p} > \bar{p}$ . Furthermore, we assume  $|\phi_{\text{id}}\rangle\langle\phi_{\text{id}}|\bar{\rho}_e = 0$  is satisfied [65,66,69]. Since  $|\phi_{\text{id}}\rangle\langle\phi_{\text{id}}|\rho_e = 0$  is also satisfied as shown in Eq. (2), the virtually purified state without normalization is defined as follows:

$$\frac{\rho\bar{\rho} + \bar{\rho}\rho}{2} = (1 - p)(1 - \bar{p})|\phi_{\text{id}}\rangle\langle\phi_{\text{id}}| + p\bar{p} \text{Tr}[\rho_e\bar{\rho}_e] \frac{\rho_e\bar{\rho}_e + \bar{\rho}_e\rho_e}{2 \text{Tr}[\rho_e\bar{\rho}_e]}, \quad (5)$$

where the state  $\rho\bar{\rho} + \bar{\rho}\rho$  is Hermitian.  $\rho\bar{\rho} + \bar{\rho}\rho$  may also not be a density matrix because this may not be a semidefinite-positive operator. However, this is called a virtually purified state in the original paper [69], and thus we adopt the same terminology as the previous study. It is worth mentioning that we cannot directly obtain the state  $\rho\bar{\rho} + \bar{\rho}\rho$  on actual devices. However, we can compute the expectation values with this state by postprocessing the measurement results, as we will explain in the next paragraph. Note that this EM method decreases the ratios between the error state and the ideal

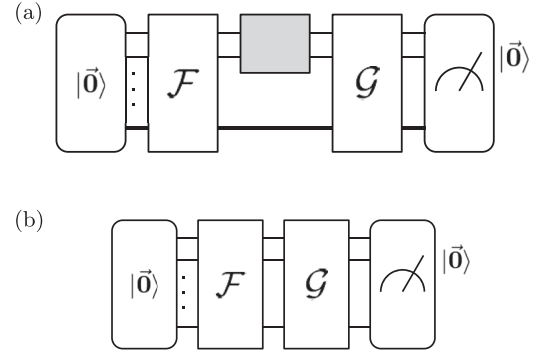


FIG. 2. Circuits for implementing dual-state purification. We calculate the numerator (denominator) in Eq. (6) with the circuit in (a) [(b)]. First, we apply a noisy map  $\mathcal{F}$  in Eq. (4) to an initial state  $|\vec{0}\rangle$ . Second, when we calculate the numerator in Eq. (6), we perform the projective measurement  $P_\sigma^\pm$  of a Pauli product  $\sigma$  (the gray box), as shown in (a). To obtain the denominator in Eq. (6) by the circuit in (b), the projective measurement is not implemented. Third, we apply a noisy inverse map  $\mathcal{G}$  in Eq. (4). Finally, we measure the state on the basis of the initial state  $|\vec{0}\rangle$ .

state from  $p/(1 - p)$  to  $p\bar{p} \text{Tr}[\rho_e\bar{\rho}_e]/(1 - p)(1 - \bar{p})$ . Moreover, we can derive the upper bound of the ratio for the EM method as  $p\bar{p} \text{Tr}[\rho_e\bar{\rho}_e]/(1 - p)(1 - \bar{p}) \leq p\bar{p}/(1 - p)(1 - \bar{p})$ . This means that the ratio of the EM method is smaller than that of the original method if  $p < 0.5$  and  $\bar{p} < 0.5$  are satisfied.

We obtain the expectation value of an observable  $O$  as  $\langle O \rangle = \sum a_i \langle \sigma_i \rangle$  by decomposing  $O$  as the summation of the expectation values of Pauli products  $\{\sigma_i\}$ , where  $a_i$  is a coefficient. Dual-state purification gives the expectation value of a Pauli product  $\sigma$  as follows:

$$\langle \sigma \rangle \simeq \text{Tr} \left[ \sigma \frac{\rho\bar{\rho} + \bar{\rho}\rho}{2} \right] / \text{Tr} \left[ \frac{\rho\bar{\rho} + \bar{\rho}\rho}{2} \right], \quad (6)$$

where  $\text{Tr}[\frac{\rho\bar{\rho} + \bar{\rho}\rho}{2}]$  denotes a normalization factor. To obtain this expectation value, we can use the quantum circuits depicted in Fig. 2. The circuit in Fig. 2(a) [Fig. 2(b)] is used to obtain the numerator (denominator) in Eq. (6). In this method, we start by preparing an initial state  $|\vec{0}\rangle$  and let it evolve through the noisy quantum circuit described by the channel  $\mathcal{F}$ . Second, we perform a measurement operator  $P_\sigma^\pm$  associated with the projective measurement of the Pauli product  $\sigma$  to obtain the numerator (the gray box), as shown in Fig. 2(a). Here, the measurement operator corresponding to the outcome  $\pm 1$  is given by  $P_\sigma^\pm = (I \pm \sigma)/2$ . To implement the projective measurement  $P_\sigma^\pm$ , we need to perform single-qubit rotations. When we implement the circuit shown in Fig. 2(b) to obtain the denominator in Eq. (6), we do not perform the projective measurement. Third, we let the state evolve by the noisy quantum process described by the channel  $\mathcal{G}$ . Finally, we investigate how much of the population remains in  $|\vec{0}\rangle$  by a measurement in the basis including  $|\vec{0}\rangle$ . If we select the circuit shown in Fig. 2(b), we can measure the denominator in Eq. (6) as follows:

$$P_0 = \langle \vec{0} | \mathcal{G}(\mathcal{F}(|\vec{0}\rangle\langle\vec{0}|)) | \vec{0} \rangle = \text{Tr}[\bar{\rho}\rho], \quad (7)$$

where  $P_{\vec{0}}$  denotes the population of  $|\vec{0}\rangle$  in the final state obtained by the measurement. Meanwhile, if we select the circuit shown in Fig. 2(a), we can measure the numerator in Eq. (6) as  $\tilde{P}_{\vec{0}}^+ - \tilde{P}_{\vec{0}}^-$ , where

$$\tilde{P}_{\vec{0}}^{\pm} = \langle \vec{0} | \mathcal{G}(P_{\sigma}^{\pm} \mathcal{F}(|\vec{0}\rangle\langle \vec{0}|) P_{\sigma}^{\pm}) | \vec{0} \rangle = \text{Tr}[P_{\sigma}^{\pm} \rho P_{\sigma}^{\pm} \bar{\rho}], \quad (8)$$

and  $\tilde{P}_{\vec{0}}^{\pm}$  denotes the population of  $|\vec{0}\rangle$ . Thus, the expectation value is rewritten as

$$\langle \sigma \rangle = (\tilde{P}_{\vec{0}}^+ - \tilde{P}_{\vec{0}}^-) / P_{\vec{0}}. \quad (9)$$

In EM, we must also suppress the sampling noise that leads to the residual error. We can decrease the variance of the expectation value in Eq. (9) by increasing the number of measurements. Owing to the denominator, the variance of Eq. (9) is larger than that of Eq. (8). In particular, when  $\text{Tr}[\bar{\rho} \rho]$  approaches 0, the variance diverges to infinity. Therefore, to implement this method within a finite time, we need a finite value of  $\text{Tr}[\bar{\rho} \rho]$ .

#### IV. ERROR-MITIGATED QUANTUM ANNEALING

In this section, we describe our QA scheme for obtaining the ground-state energy of a problem Hamiltonian by mitigating the environmental noise effects. To adapt the EM method mentioned in the previous section to QA, we design a QA schedule to construct the operations  $\mathcal{F}$  and  $\mathcal{G}$ . We refer to this approach as error-mitigated quantum annealing (EMQA). As we mentioned in the previous section, the inverse map  $\mathcal{G}$  should meet  $\mathcal{G}(\bullet) = U^{\dagger} \bullet U$  when there is no decoherence. EMQA is designed to satisfy this condition. As long as this condition is satisfied, the dual-state purification lets us measure the expectation value accurately even under the effect of noise, as we explained in the previous section. We show that this approach provides a more accurate estimation of the energy than that provided by the conventional approach.

EMQA is expressed as

$$H_{\text{EMQA}}(t) = A_{\text{EMQA}}(t)H_{\text{D}} + B_{\text{EMQA}}(t)H_{\text{P}}, \quad (10)$$

$$A_{\text{EMQA}}(t) = \begin{cases} -\frac{t}{T} + 1 & (t : 0 \rightarrow T), \\ 0 & (t : T \rightarrow T + T'), \\ -\frac{t}{T} + \frac{T'}{T} + 1 & (t : T + T' \rightarrow 2T + T'), \end{cases} \quad (11)$$

$$B_{\text{EMQA}}(t) = \begin{cases} \frac{t}{T} & (t : 0 \rightarrow T), \\ -\frac{2t}{T'} + \frac{2T}{T'} + 1 & (t : T \rightarrow T + T'), \\ \frac{t}{T} - \frac{T'}{T} - 2 & (t : T + T' \rightarrow 2T + T'). \end{cases} \quad (12)$$

This schedule is shown in Fig. 3. From  $t = T$  to  $T + T'$ , we turn off the driver Hamiltonian. Since we only change the amplitude of the problem Hamiltonian, the nonadiabatic transitions do not occur. On the other hand, if there is decoherence from the environment, we should change the sign of the problem Hamiltonian instantaneously. However, it is difficult to implement such an immediate change in the sign of the

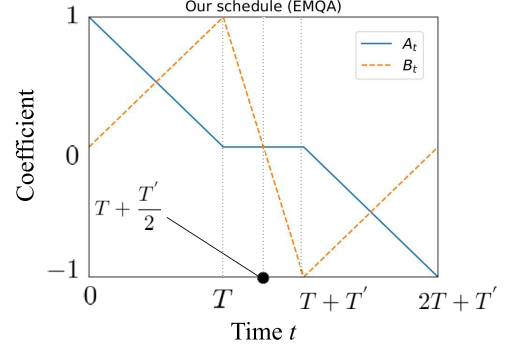


FIG. 3. QA schedule for implementing dual-state purification. The dynamics from  $t = 0$  to  $T + T'/2$  corresponds to the noisy map  $\mathcal{F}$ , and this schedule from  $t = T + T'/2$  to  $2T + T'$  provides the dynamics corresponding to the inverse map  $\mathcal{G}$  in Eq. (4). To calculate the numerator in Eq. (6), a projective measurement is required at  $t = T + T'/2$ .

Hamiltonian for QA devices. Therefore, we keep the time as short as possible within the bandwidth of the devices. Again, to obtain the numerator of Eq. (9), we must perform a projective measurement  $P_{\sigma}^{\pm}$  at  $t = T + T'/2$ . Thus, the dynamics from  $t = 0$  to  $T + T'/2$  represents the map  $\mathcal{F}$ , whereas the dynamics from  $t = T + T'/2$  to  $2T + T'$  corresponds to the inverse map  $\mathcal{G}$ . In Appendix A, we show that the time evolution from  $t = T + T'/2$  to  $2T + T'$  is equivalent to the conjugate transpose of the dynamics from  $t = 0$  to  $T + T'/2$  when there is no decoherence, even if the adiabatic condition is not satisfied.

To consider the decoherence, we employ the Gorini-Kossakowski-Sudarshan-Lindblad (GKSL) master equation to describe the dynamics of the system [113,114]:

$$\frac{d\rho}{dt} = -i[H(t), \rho] + \sum_n \frac{\lambda_n}{2} (2\hat{L}_n \rho \hat{L}_n^{\dagger} - \{\hat{L}_n^{\dagger} \hat{L}_n, \rho\}), \quad (13)$$

where  $[\bullet, \bullet]$  denotes the commutator,  $\lambda_n$  denotes the decay rate,  $\hat{L}_n$  denotes the Lindblad operator,  $\{\bullet, \bullet\}$  denotes the anticommutator, and  $H(t)$  denotes  $H_{\text{CQA}}(t)$  or  $H_{\text{EMQA}}(t)$ .

Throughout this paper, we assume that we can realize the dynamics induced by the Hamiltonian and arbitrary single-qubit rotations, and projective measurements. Owing to the recent development of quantum technologies, such a device is feasible, which we will discuss later. However, it is unclear whether we can implement two-qubit gates with high fidelity. To perform two-qubit gates, one should quickly change the interaction Hamiltonian and/or should perform complicated pulse operations. For these reasons, the infidelity of the two-qubit gates is usually much larger than that of the single-qubit gates [32]. Hence, we assume that we cannot apply two-qubit gates to the devices. This assumption is similar to that of digital-analog quantum computation (DAQC) [115]. This approach has been proposed as a hybrid architecture to achieve flexible NISQ computation on robust analog quantum simulators.

It is worth noting that dual-state purification is more suitable for the device considered here than virtual distillation. Although virtual distillation is also an efficient method for suppressing stochastic errors, it requires two-qubit gates to

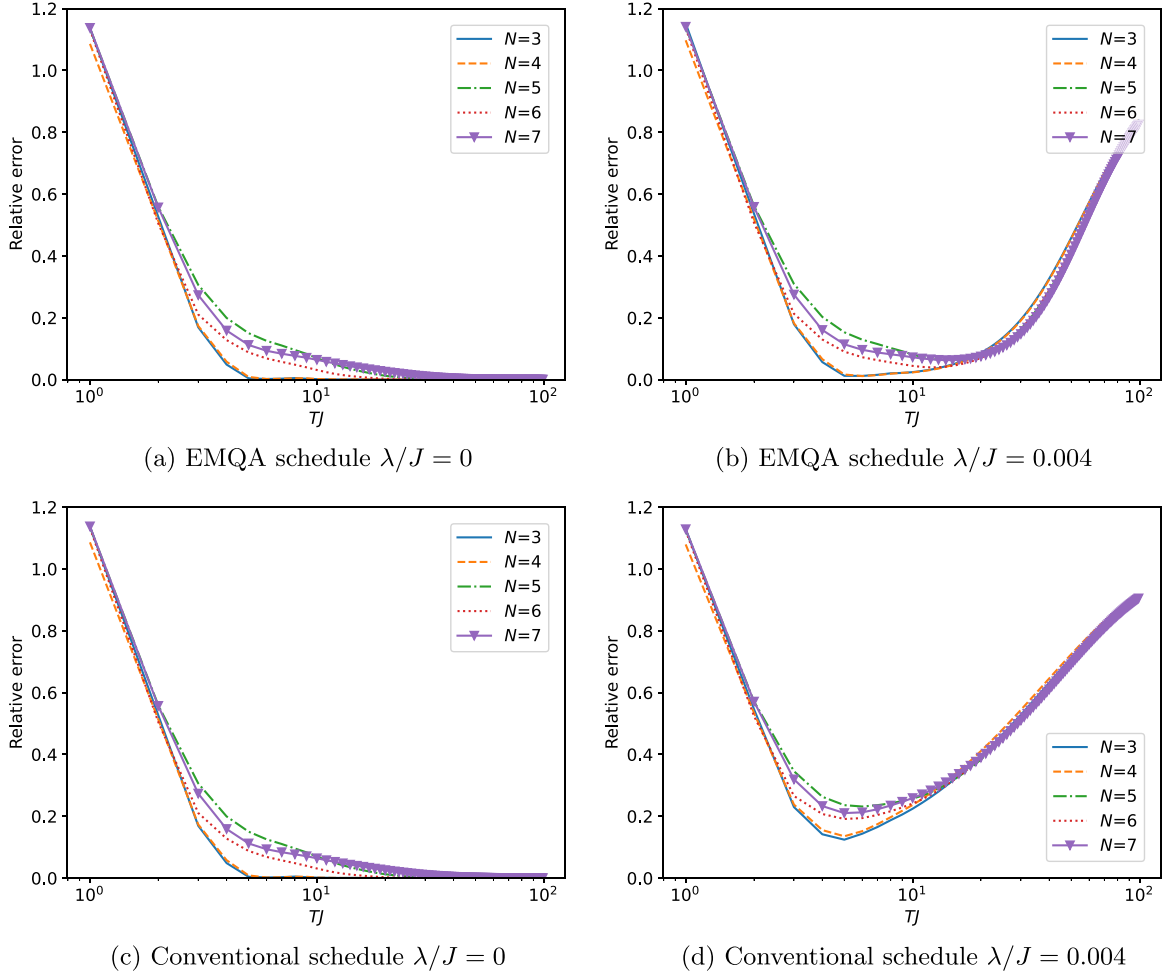


FIG. 4. Relative error of the ground-state energy of the problem Hamiltonian  $H_p$ . We define the relative error as  $(\langle H_p \rangle - E_g)/|E_g|$ , where  $\langle H_p \rangle$  denotes the expectation value with QA and  $E_g$  denotes the actual value of the ground-state energy. We adopt (a) the EMQA and (c) the conventional schedule with  $\lambda = 0$ . In addition, we adopt (b) the EMQA and (d) the conventional schedule with  $\lambda/J = 0.004$ . The annealing time  $T$  is normalized by  $J$ . We show that the EMQA schedule provides a minimum error that is lower than that of the conventional method for all  $N$  (see Table I).

entangle  $M$  copies of a noisy state  $\rho$ . Thus, it is not straightforward to implement virtual distillation under our assumption. Meanwhile, in dual-state purification, we do not prepare  $M$  copies of a noisy state  $\rho$  or implement two-qubit gates as mentioned in the previous section. Thus, EMQA is more practical for mitigating the noise effects during QA.

## V. RESULTS

In this section, we demonstrate the performance of the EMQA schedule and compare it with that of the conventional schedule. For this purpose, we consider the problem Hamiltonian as the Heisenberg model expressed as

$$H_p = J \sum_{i=1}^N (\hat{\sigma}_i^x \hat{\sigma}_{i+1}^x + \hat{\sigma}_i^y \hat{\sigma}_{i+1}^y + \Delta \hat{\sigma}_i^z \hat{\sigma}_{i+1}^z) \quad (14)$$

with the periodic boundary condition, where  $J$  and  $\Delta$  are coefficients. Throughout this paper, by setting  $J = 2\pi \times 100$  MHz, the time and energy are normalized by this value. This is the typical value for actual experiments [116]. To

simplify the discussion, we select the Lindblad operators as the Pauli matrices  $\hat{\sigma}_i^x$ ,  $\hat{\sigma}_i^y$ , and  $\hat{\sigma}_i^z$ , and we assume that the decay rate is constant regardless of the index (i.e.,  $\lambda_n = \lambda$ ). In our numerical simulation, the GKSL master equation is rewritten as

$$\frac{d\rho}{dt} = -i[H(t), \rho] - \frac{\lambda}{2} \sum_{i=1}^N \sum_{j \in \{x,y,z\}} [\hat{\sigma}_i^j, [\hat{\sigma}_i^j, \rho]]. \quad (15)$$

Furthermore, we set  $B/J = 1$ ,  $T'J = 5$ , and  $\Delta = -1$ . To evaluate the performances of these schedules, we define a relative error as  $(\langle H_p \rangle - E_g)/|E_g|$ , where  $\langle H_p \rangle$  is the expectation value of the problem Hamiltonian obtained through the numerical simulations and  $E_g$  denotes the ground-state energy of the problem Hamiltonian.

We plot the relative error against the parameter  $T$  by changing the number of qubits  $N$  in Fig. 4. We prepare a set of the annealing time  $T$  beforehand and implement QA with each annealing time. It means that we can minimize the expectation value of  $H_p$  by choosing the most suitable annealing time. This strategy is effective especially when the problem

TABLE I. Minimum expectation values, the relative error, the optimal annealing time  $T$  to minimize the energy, and the exact value of the ground-state energy. Here, we normalize the energy by  $J$  (i.e.,  $\langle H_p \rangle / J$ ), and we set  $J = 2\pi \times 100$  MHz for the optimal annealing time. We set  $T'/J = 5$  in EMQA in all cases.

Expectation value, relative error, and annealing time $T$ (ns) when $\lambda/J = 0.004$			
	EMQA	Conventional	Exact
$N = 3$	-2.96, 0.0119, 9.55 ns	-2.63, 0.124, 7.96 ns	-3.00
$N = 4$	-3.95, 0.0114, 9.55 ns	-3.46, 0.135, 7.96 ns	-4.00
$N = 5$	-4.69, 0.0624, 23.9 ns	-3.84, 0.231, 9.55 ns	-5.00
$N = 6$	-5.76, 0.0395, 19.1 ns	-4.85, 0.191, 7.96 ns	-6.00
$N = 7$	-6.56, 0.0630, 22.3 ns	-5.53, 0.210, 7.96 ns	-7.00

Hamiltonian is nondiagonal [111,117]. The reason why we can see such a minimal point is that as we increase  $T$ , the decoherence becomes more relevant whereas the nonadiabatic transitions become less significant. The minimum expectation values and the relative errors obtained through the numerical simulations are listed in Table I.

Figure 4(a) shows the result of the numerical simulation using the EMQA schedule with  $\lambda = 0$ . We check that the relative errors converge to zero regardless of the number of qubits when no decoherence occurs. In this case,  $\frac{\rho\bar{\rho} + \bar{\rho}\rho}{2} = |\phi_{id}\rangle\langle\phi_{id}|$  and  $\text{Tr}[\rho\bar{\rho}] = 1$ . This state is the same as that obtained by the conventional QA except for the relative phase coming from the dynamics from  $T$  to  $T + T'$ . This relative phase does not affect the estimation of the ground-state energy. Thus, we can see the same results with the EMQA and the conventional QA in Figs. 4(a) and 4(c). In addition, we show that even under the effect of decoherence with  $\lambda/J = 0.004$ , we can obtain a more accurate estimation of the ground-state energy than that obtained using the conventional method, as shown in Table I.

In Fig. 5, we also compare the performance of our method with that of the conventional one for several decay rates  $\lambda$  with  $N = 7$ . Similar to the results in Fig. 4, we can minimize the relative error to choose the optimize the annealing time for each  $\lambda$ . Figure 5(a) [5(b)] represents how the minimized

relative error (the annealing time) increases (decreases) as  $\lambda$  increases. Figure 5(a) illustrates that the conventional QA leads to larger relative errors, even when the noise effect is weak. In contrast, EMQA suppresses the impact of the noise significantly. In Fig. 5(b), the optimal annealing time of the conventional method is smaller than that of our method. This comes from the fact that we can suppress decoherence with our method, so we can set a larger annealing time to avoid nonadiabatic transitions.

Finally, we discuss the physical implementation of our scheme. We can use superconducting flux qubits (or capacitively shunted flux qubits) for both QA and gate-type quantum computation [99]. Furthermore, the Hamiltonian of the Heisenberg model with transverse fields can be realized using these systems [118]. For these systems, the thermal excitation time can be as long as tens of microseconds [119], and the coupling strength can be tens of MHz or higher [116]. Thus, by using these quantum devices, we can realize  $J/\lambda \simeq 10^3$ , which is similar to those used in our simulations. Also, when we use the superconducting flux qubits, we can tune the coupling strength and magnetic fields by changing the magnetic flux penetrating the SQUID structure [120–122], and thus we can realize the linear scheduling in Eq. (10) by applying a suitable magnetic flux. Therefore, these systems are candidates for realizing our proposal.

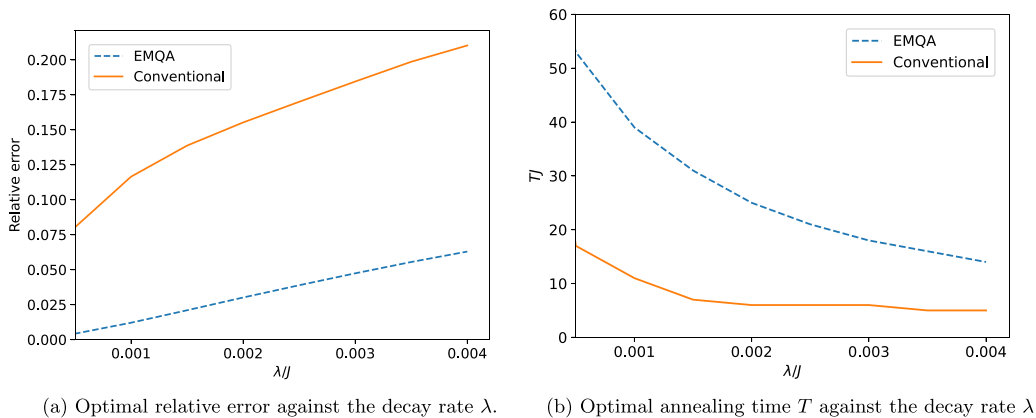


FIG. 5. Minimized relative error (a) and the optimized annealing time (b) for several decay rates  $\lambda$  with  $N = 7$ . (a) Shows the relative error with our method is much smaller than that of the conventional one for all  $\lambda$ . (b) Indicates that our method allows us to set a longer annealing time than the conventional one for all  $\lambda$ . This comes from the fact that we can set longer annealing times due to the decoherence suppression, which allows us to avoid the nonadiabatic transitions.

## VI. CONCLUSION

We proposed a QA strategy combined with an EM method for suppressing the effects of decoherence. Among the various EM methods, we adopted dual-state purification, which does not require two-qubit gates and is hence suitable for the devices developed for QA. Our protocol consists of four steps. First, we let the system evolve by the Hamiltonian. Second, we perform single-qubit projective measurements. Third, we let the system evolve by the Hamiltonian whose dynamics corresponds to an inverse map of the first dynamics. Finally, we postprocess the measurement results. We numerically showed that the ground-state energy estimated using our protocol is more accurate than that estimated using the conventional QA under decoherence.

Throughout our paper, we only consider incoherent errors coming from decoherence. On actual devices, we might also face coherent errors caused by imperfect linear scheduling. Randomized compiling is an efficient method to convert coherent errors into incoherent ones [123]. It is future work to examine whether we can adopt randomized compiling to our scheme.

## ACKNOWLEDGMENTS

We are grateful to S. Endo, K. Yamamoto, H. Hakoshima, T. Imoto, and N. Yoshioka for their valuable advice. This work was supported by the Leading Initiative for Excellent Young Researchers, MEXT, Japan, and JST Presto (Grant No. JPMJPR1919) Japan. This paper is partly based on the results obtained from a project, JPNP16007, commissioned by the New Energy and Industrial Technology Development Organization (NEDO), Japan. This work was supported by JST Moonshot R&D (Grant No. JPMJMS226C). Y.M. is supported by JSPS KAKENHI (Grant No. 23H04390). The numerical simulations shown in Fig. 4 were performed using QUTIP, an efficient framework for simulating quantum mechanics [124].

## APPENDIX A: PROOF FOR INVERSE MAP IN EMQA SCHEDULE

For dual-state purification, we must construct an inverse transformation of the target unitary dynamics. Here, we show that, with the EMQA schedule, the dynamics from  $t = T + T'/2$  to  $2T + T'$  is equivalent to the conjugate transpose of the dynamics from  $t = 0$  to  $T + T'/2$  when no decoherence occurs.

First, the dynamics from  $t = T + T'/2$  to  $T + T'$  is equivalent to the conjugate transpose of the dynamics from  $t = T$  to  $T + T'/2$ , i.e.,

$$\begin{aligned} U\left(T + \frac{T'}{2}, T + T'\right) &= \exp\left(-i \int_{T+T'/2}^{T+T'} B_{\text{EMQA}}(t) H_P dt\right) = \exp\left(i H_P \frac{T'}{4}\right) \\ &= \exp\left(-i \int_T^{T+T'/2} B_{\text{EMQA}}(t) H_P dt\right)^\dagger \\ &= U\left(T, T + \frac{T'}{2}\right)^\dagger, \end{aligned} \quad (\text{A1})$$

where  $U(t', t) = \mathcal{T} \exp(-i \int_t^{t'} d\tau H_{\text{EMQA}}(\tau))$ .

Next, let us consider the dynamics from  $t = T + T'$  to  $2T + T'$ . By transforming the variable  $t$  ( $t : T + T' \rightarrow 2T + T'$ ) into a variable  $s$  ( $s : 0 \rightarrow T$ ) by  $t = s + T + T'$ , we obtain

$$H_2(s) = -\frac{s}{T} H_D + \left(\frac{s}{T} - 1\right) H_P. \quad (\text{A2})$$

Thus, using the Trotter decomposition, we can express the dynamics of the Hamiltonian  $H_2(s)$  as follows:

$$\begin{aligned} \mathcal{T} \exp\left(-i \int_0^T H_2(s) ds\right) &\simeq \exp(-i H_2(M\delta t)\delta t) \exp(-i H_2((M-1)\delta t)\delta t) \dots \\ &\quad \times \exp(-i H_2(\delta t)\delta t) \exp(-i H_2(0)\delta t) \\ &= \prod_{j=0}^M \exp(-i H_2(j\delta t)\delta t), \end{aligned} \quad (\text{A3})$$

where  $\mathcal{T}$  denotes the time-ordered product,  $M$  denotes a natural number, and  $\delta t = T/M$  denotes a discretized time. Note that  $\mathcal{T} \exp[-i \int_0^T H_2(s) ds]$  is equal to the second line in the limit of a small  $\delta t$ . Meanwhile, we define the time-dependent Hamiltonian from  $t = 0$  to  $T$  as

$$H_1(t) = \left(1 - \frac{t}{T}\right) H_D + \frac{t}{T} H_P. \quad (\text{A4})$$

We can decompose the conjugate transpose of the dynamics from  $t = 0$  to  $T$  as

$$\begin{aligned} \left[\mathcal{T} \exp\left(-i \int_0^T H_1(t) dt\right)\right]^\dagger &\simeq (\exp(-i H_1(M\delta t)\delta t) \exp[-i H_1((M-1)\delta t)\delta t] \dots \\ &\quad \times \exp(-i H_1(\delta t)\delta t) \exp(-i H_1(0)\delta t))^\dagger \\ &= \exp(i H_1(0)\delta t) \exp(i H_1(\delta t)\delta t) \dots \\ &\quad \times \exp[i H_1((M-1)\delta t)\delta t] \exp(i H_1(M\delta t)\delta t) \\ &= \prod_{j=0}^M \exp[i H_1((M-j)\delta t)\delta t]. \end{aligned} \quad (\text{A5})$$

As  $\exp(-i H_2(j\delta t)\delta t) = \exp(i H_1((M-j)\delta t)\delta t)$  is satisfied for each index  $j$ , we have

$$\begin{aligned} U(T + T', 2T + T') &= \mathcal{T} \exp\left(-i \int_0^T H_2(s) ds\right) \\ &= \prod_{j=0}^{\infty} \exp(-i H_2(j\delta t)\delta t) = \prod_{j=0}^{\infty} \exp(i H_1((M-j)\delta t)\delta t) \\ &= \left[\mathcal{T} \exp\left(-i \int_0^T H_1(t) dt\right)\right]^\dagger = U(0, T)^\dagger. \end{aligned} \quad (\text{A6})$$



Therefore, using Eqs. (A1) and (A6), we show that

$$\begin{aligned}
 & U\left(T + \frac{T'}{2}, 2T + T'\right) \\
 &= U(T + T', 2T + T')U\left(T + \frac{T'}{2}, T + T'\right) \\
 &= U(0, T)^\dagger U\left(T, T + \frac{T'}{2}\right)^\dagger \\
 &= U\left(0, T + \frac{T'}{2}\right)^\dagger. \tag{A7}
 \end{aligned}$$

**APPENDIX B: RQA-BASED SCHEDULE**

Let us explain a naive schedule inspired by reverse quantum annealing (RQA) [125–130]. First, we change the total Hamiltonian from  $H_P$  to  $H_D$ . Second, we bring back the Hamiltonian to  $H_P$ . If there is neither decoherence nor nonadiabatic transitions, in the first step, the quantum state evolves from the initial state to the ground state of  $H_P$ , and in the second step, the quantum state evolves to the final state close to the initial state. Thus, in this ideal case, the first step provides  $U$  while the second step seems to provide  $U^\dagger$  [125–130]. It means that RQA is a candidate to provide the inverse map. However, this schedule cannot purify the noisy state if nonadiabatic transitions occur. It is worth mentioning that, in the dual-state purification, we use a classical computer for postprocessing the measurement results, and estimate the expectation value of the observable. The corresponding density matrix, which is not directly generated on a quantum computer, can be unphysical due to the artifact of the post-processing when using this schedule.

Let us demonstrate the RQA-based schedule. The total Hamiltonian and the coefficients are written as

$$H_{\text{RQA}}(t) = A_{\text{RQA}}(t)H_D + B_{\text{RQA}}(t)H_P, \tag{B1}$$

$$A_{\text{RQA}}(t) = \begin{cases} -\frac{t}{T} + 1 & (t : 0 \rightarrow T), \\ \frac{t}{T} - 1 & (t : T \rightarrow 2T), \end{cases} \tag{B2}$$

$$B_{\text{RQA}}(t) = \begin{cases} \frac{t}{T} & (t : 0 \rightarrow T), \\ -\frac{t}{T} + 2 & (t : T \rightarrow 2T). \end{cases} \tag{B3}$$

This annealing schedule is shown in Fig. 6. To obtain the numerator of Eq. (9) with dual-state purification, we must implement a projective measurement  $P_\sigma^\pm$  at  $t = T$ . The dynamics from  $t = 0$  to  $T$  corresponds to the map  $\mathcal{F}$ , whereas the dynamics from  $t = T$  to  $2T$  corresponds to the inverse map  $\mathcal{G}$ . Here, we consider a specific case in which the following three conditions are satisfied. First, the adiabatic condition is satisfied. Second, the initial state is the ground state of the driver Hamiltonian. Third, no decoherence occurs. If these conditions are satisfied, the final state returns to the initial state. This seems to indicate that the RQA-based schedule provides the inverse map, and dual-state purification using this schedule may be feasible in practical circumstances. However, we show that, if nonadiabatic transitions occur, the RQA-based schedule does not provide the proper inverse map. In

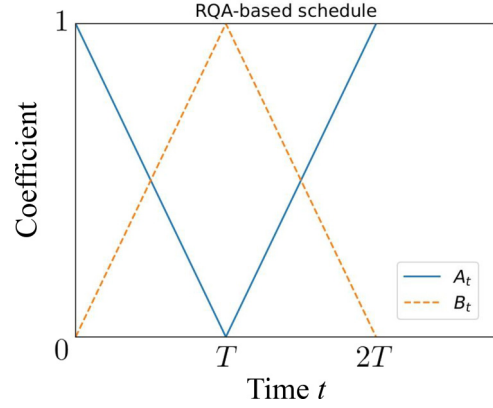


FIG. 6. Schedule inspired by RQA. The dynamics from  $t = 0$  to  $T$  ( $t = T$  to  $2T$ ) corresponds to the noisy map  $\mathcal{F}$  ( $\mathcal{G}$ ) in Eq. (4). At  $t = T$ , we perform a projective measurement to calculate the numerator in Eq. (6). In Appendix B, we show that we cannot accurately estimate the ground-state energy of  $H_P$  using this schedule.

this schedule, the virtually obtained state described by Eq. (5) can be unphysical because the energy of the state can be lower than the ground-state energy of the problem Hamiltonian. We explain the origin of this unphysicality using both analytical and numerical methods.

Figures 7(a) and 7(b) show the performance of the method using the RQA-based schedule. Regardless of the number of qubits, the minimum expectation values are lower than the ground-state energies, as shown in Table II. If we calculate the energy using  $\text{Tr}[\rho H_P]$ , we always have  $\text{Tr}[\rho H_P] \geq E_g$ , where  $\rho$  denotes an arbitrary density matrix. Thus, the method with the RQA-based schedule provides us with an unphysical state. In this case, even if we minimize the expectation value of the energy by changing  $T$ , the minimized value is not always the closest to the actual value, which is a significant disadvantage of using the method with the RQA-based schedule. In Figs. 7(a) and 7(b), we can see the irregular behavior. Since we cannot construct the strict inverse map, the nonadiabatic transitions occur, and a combinational effect of relative phase and nonadiabatic transitions occurs in the state. We consider that this is the reason for the irregular behavior. In Appendix C, we

TABLE II. Minimum expectation values, the relative error, the optimal annealing time to minimize the energy, and the exact value of the ground-state energy. Here, we normalize the energy by  $J$  (i.e.,  $\langle H_P \rangle / J$ ), and we set  $J = 2\pi \times 100$  MHz for the optimal annealing time.

Expectation value, relative error, and annealing time (ns) when $\lambda/J = 0.004$				
	RQA-based			Exact
$N = 3$	-3.41,	-0.138,	4.77 ns	-3.00
$N = 4$	-5.32,	-0.329,	3.18 ns	-4.00
$N = 5$	-5.83,	-0.167,	9.55 ns	-5.00
$N = 6$	-17.2,	-1.87,	3.18 ns	-6.00

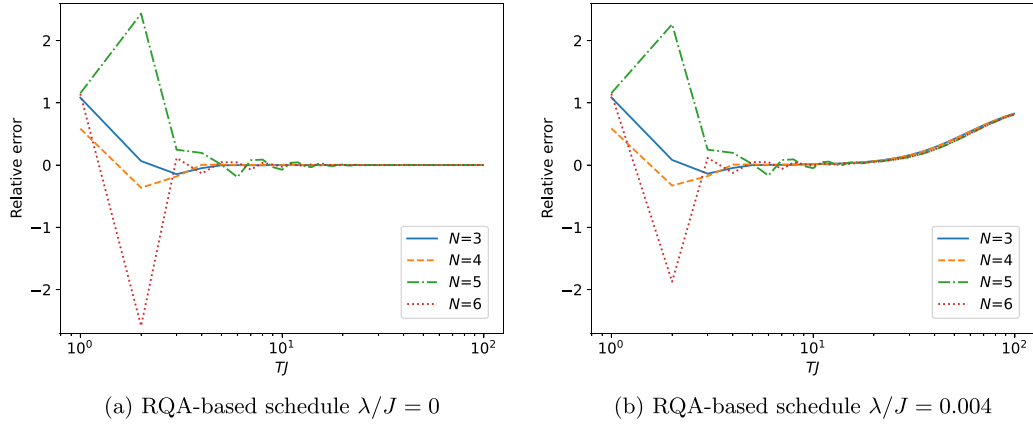


FIG. 7. Relative error of the ground-state energy of the problem Hamiltonian  $H_p$ . We define the relative error as  $(\langle H_p \rangle - E_g)/|E_g|$ , where  $\langle H_p \rangle$  denotes the expectation value with QA and  $E_g$  denotes the actual value of the ground-state energy. We adopt the RQA-based schedule with  $\lambda/J = 0$  and  $0.004$  in (a) and (b), respectively. The annealing time  $T$  is normalized by  $J$ . We show that the relative error with the RQA-based schedule can be lower than zero at some  $T$  for all  $N$ . Thus, the RQA-based schedule may produce unphysical results where the corresponding density matrix has negative eigenvalues.

analytically show an example that the RQA-based schedule actually provides an unphysical state by using a simple model.

### APPENDIX C: THEORETICAL ANALYSIS OF RQA-BASED SCHEDULE

In Appendix B, we noted that the expectation value of  $H_p$  becomes lower than the ground-state energy in the case of the RQA-based method in the numerical simulations. To better understand this phenomenon, we derive the analytic expressions of the RQA-based method with a single qubit. We will show that, for this case, the state  $\rho\bar{\rho} + \bar{\rho}\rho$  becomes unphysical in the sense that the eigenvalues of this state become lower than 0 unlike the physical density matrices. In this Appendix, we do not consider the effect of decoherence, as we can observe such an unphysical situation even if there is no decoherence, as shown in Fig. 7(a). We redefine the time-dependent Hamiltonian from  $t = 0$  to  $T$  for the QA as follows:

$$H_{\text{RQA}}(t) = -\sin\left(\frac{\pi t}{2T}\right)\hat{\sigma}^z - \cos\left(\frac{\pi t}{2T}\right)\hat{\sigma}^x. \quad (\text{C1})$$

We can diagonalize this Hamiltonian using a unitary matrix that is expressed as

$$V(t) = \begin{pmatrix} \cos\left(\frac{\pi(t+T)}{4T}\right) & -\sin\left(\frac{\pi(t+T)}{4T}\right) \\ \sin\left(\frac{\pi(t+T)}{4T}\right) & \cos\left(\frac{\pi(t+T)}{4T}\right) \end{pmatrix}. \quad (\text{C2})$$

We obtain a diagonalized matrix as follows:

$$D \equiv V(t)H_{\text{RQA}}(t)V^\dagger(t) = \begin{pmatrix} 1 & 0 \\ 0 & -1 \end{pmatrix}. \quad (\text{C3})$$

By using the matrices  $V(t)$  and  $D$ , we define an effective Hamiltonian as

$$H_{\text{eff}} = i\frac{dV(t)}{dt}V^\dagger(t) + D = \begin{pmatrix} 1 & -\frac{i\pi}{4T} \\ \frac{i\pi}{4T} & -1 \end{pmatrix}. \quad (\text{C4})$$

If no decoherence occurs, the time-evolved state  $|\psi(T)\rangle$  with the Hamiltonian  $H_{\text{RQA}}(t)$  from the initial state  $|+\rangle$  is expressed as

$$\begin{aligned} |\psi(T)\rangle &= \mathcal{T} \exp\left(-i \int_0^T H_{\text{RQA}}(t) dt\right) |+\rangle \\ &= V^\dagger(T) \exp(-iT H_{\text{eff}}) V(0) |+\rangle \\ &= \begin{pmatrix} \cos\left(\frac{1}{4}\sqrt{\pi^2 + 16T^2}\right) + \frac{4iT \sin\left(\frac{1}{4}\sqrt{\pi^2 + 16T^2}\right)}{\sqrt{\pi^2 + 16T^2}} \\ \frac{\pi \sin\left(\frac{1}{4}\sqrt{\pi^2 + 16T^2}\right)}{\sqrt{\pi^2 + 16T^2}} \end{pmatrix}. \end{aligned} \quad (\text{C5})$$

In this case, we obtain the density matrix  $\rho$  as  $|\psi(T)\rangle\langle\psi(T)|$ .

Meanwhile, the time-dependent Hamiltonian from  $t = T$  to  $2T$ , which corresponds to the inverse map  $\mathcal{G}$ , is defined as

$$H_{\text{RQA}}(t) = -\cos\left(\frac{\pi}{2T}(t-T)\right)\hat{\sigma}^z - \sin\left(\frac{\pi}{2T}(t-T)\right)\hat{\sigma}^x. \quad (\text{C6})$$

We can also diagonalize this Hamiltonian using a unitary matrix that is expressed as

$$U(t) = \begin{pmatrix} \sin\left(\frac{\pi(t-T)}{4T}\right) & -\cos\left(\frac{\pi(t-T)}{4T}\right) \\ \cos\left(\frac{\pi(t-T)}{4T}\right) & \sin\left(\frac{\pi(t-T)}{4T}\right) \end{pmatrix}. \quad (\text{C7})$$

We obtain an effective Hamiltonian for this time range as

$$H'_{\text{eff}} = i \frac{dU(t)}{dt} U(t)^\dagger + D = \begin{pmatrix} 1 & \frac{i\pi}{4T} \\ -\frac{i\pi}{4T} & -1 \end{pmatrix} \quad (\text{C8})$$

because the diagonalized matrix of the Hamiltonian in Eq. (C6) is also  $D$ . Using this effective Hamiltonian, we define a state  $|\phi(T)\rangle$  as

$$\begin{aligned} |\phi(T)\rangle &= \left[ \mathcal{T} \exp \left( -i \int_T^{2T} H_{\text{RQA}}(t) dt \right) \right]^\dagger |+\rangle \\ &= (U(2T)^\dagger \exp(-iT H'_{\text{eff}}) U(T))^\dagger |+\rangle \\ &= \begin{pmatrix} \cos\left(\frac{1}{4}\sqrt{\pi^2 + 16T^2}\right) - \frac{4iT \sin\left(\frac{1}{4}\sqrt{\pi^2 + 16T^2}\right)}{\sqrt{\pi^2 + 16T^2}} \\ \frac{\pi \sin\left(\frac{1}{4}\sqrt{\pi^2 + 16T^2}\right)}{\sqrt{\pi^2 + 16T^2}} \end{pmatrix}. \end{aligned} \quad (\text{C9})$$

Using this state, we have  $\bar{\rho}$  in Eq. (4) as  $|\phi(T)\rangle\langle\phi(T)|$ . For our purpose, it is sufficient to consider only  $\rho\bar{\rho} + \bar{\rho}\rho$  because  $\text{Tr}[\rho\bar{\rho} + \bar{\rho}\rho] > 0$  is satisfied in this case. We obtain the minimum eigenvalue  $\lambda_{\min}(T)$  of the state  $\rho\bar{\rho} + \bar{\rho}\rho$  as

$$\lambda_{\min}(T) = \frac{A - (\pi^2 + 16T^2)\sqrt{A}}{(\pi^2 + 16T^2)^2}, \quad (\text{C10})$$

where

$$\begin{aligned} A &= \pi^4 + 8\pi^2 T^2 + 256T^4 + 32\pi^2 T^2 \cos\left(\frac{1}{2}\sqrt{\pi^2 + 16T^2}\right) \\ &\quad - 8\pi^2 T^2 \cos(\sqrt{\pi^2 + 16T^2}). \end{aligned} \quad (\text{C11})$$

We plot  $\lambda_{\min}(T)$  against the parameter  $T$  in Fig. 8(a). As can be seen in Fig. 8(a),  $\lambda_{\min}(T)$  can be negative for some  $T$ . Thus, the state  $\rho\bar{\rho} + \bar{\rho}\rho$  is unphysical in the sense that the eigenvalue is negative, even if we normalize this state. As long as the state  $\rho\bar{\rho} + \bar{\rho}\rho$  has a negative eigenvalue, the expectation values of the energy  $\text{Tr}[H_{\text{P}}(\rho\bar{\rho} + \bar{\rho}\rho)]/\text{Tr}[\rho\bar{\rho} + \bar{\rho}\rho]$  will be lower than the ground-state energy.

We expect this negative eigenvalue of  $\rho\bar{\rho} + \bar{\rho}\rho$  to be related to the nonadiabatic transitions during QA. Actually, we confirm that the unphysical state appears at relatively small  $T$ , as shown in Fig. 7(a). For further investigation, we define a transition rate  $P(T)$  as

$$P(T) = |\langle 1 | \psi(T) \rangle|^2 = \frac{\pi^2 \sin^2\left(\frac{\sqrt{\pi^2 + 16T^2}}{4}\right)}{\pi^2 + 16T^2}. \quad (\text{C12})$$

When  $P(T)$  is not zero, non-adiabatic transitions occur during the dynamics. Using the transition rate  $P(T)$ , we have

$$\lambda_{\min}(T) = \left( \sqrt{1 - \frac{64T^2 P(T)^2}{\pi^2}} - \frac{1}{2} \right)^2 - \frac{1}{4}. \quad (\text{C13})$$

We plot  $T^2 P(T)^2$  against the parameter  $T$  in Fig. 8(b). Further, we confirm that the eigenvalue  $\lambda_{\min}(T)$  decreases (increases) as  $T^2 P(T)^2$  increases (decreases) in Fig. 8. Thus, the nonadiabatic transitions are closely related to the negative eigenvalues of the state  $\rho\bar{\rho} + \bar{\rho}\rho$  in Eq. (C13).

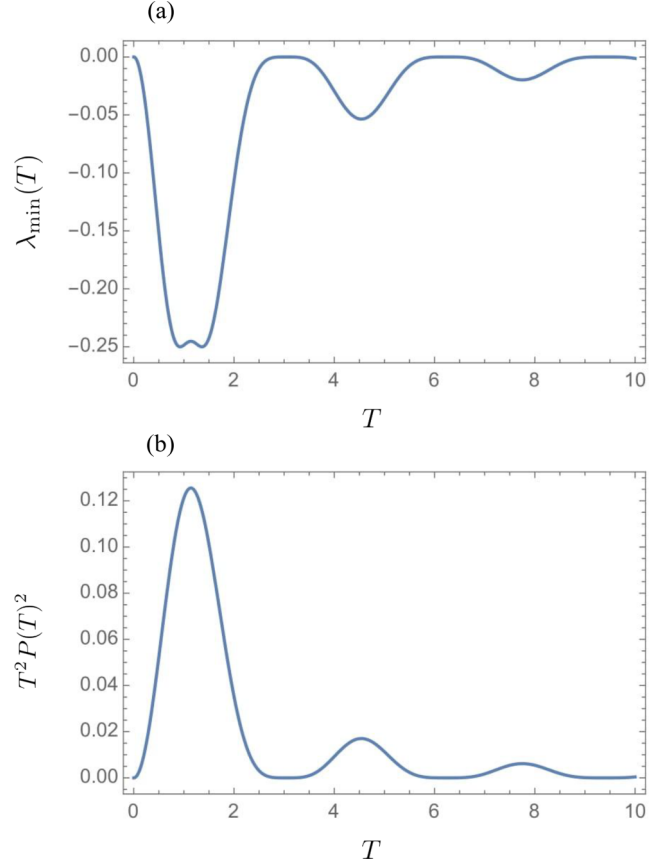


FIG. 8. Relationship between the transition rate  $P(T)$  in Eq. (C12) and the minimum eigenvalue  $\lambda_{\min}(T)$  in Eq. (C10) of the state  $\rho\bar{\rho} + \bar{\rho}\rho$ . We plot  $\lambda_{\min}(T)$  and  $T^2 P(T)^2$  against the annealing time  $T$  in (a) and (b), respectively. We check that they have peaks at the same points of  $T$ . This serves as evidence of the eigenvalue being closely related to the nonadiabatic transition, as shown by Eq. (C13).

#### APPENDIX D: ESTIMATION OF $p$ AND $\bar{p}$

To understand the improvement by EMQA in Fig. 4, here we calculate the values of  $p$  and  $\bar{p}$  in Eq. (5) in numerical simulation. We denote the noisy map defined by the time evolution according to Eq. (15) with EMQA from  $t = a$  to  $b$  as  $\mathcal{F}_a^b$ . As we discussed in Sec. III, the quantum state  $\rho$  after the time evolution from  $t = 0$  to  $T + T'/2$  is described as

$$\mathcal{F}_0^{T+T'/2}(|+\rangle\langle+|^{\otimes N}) = (1-p)|\phi_{\text{id}}\rangle\langle\phi_{\text{id}}| + p\rho_e, \quad (\text{D1})$$

where  $|\phi_{\text{id}}\rangle = U(0, T + T'/2)|+\rangle^{\otimes N}$  and  $\rho_e |\phi_{\text{id}}\rangle = 0$ .  $U(t', t)$  is defined in Eq. (A1). Thus, we can numerically compute

$$p = 1 - \langle\phi_{\text{id}}|\mathcal{F}_0^{T+T'/2}(|+\rangle\langle+|^{\otimes N})|\phi_{\text{id}}\rangle. \quad (\text{D2})$$

Let us consider the dual state  $\bar{\rho}$  described by the dual map of the noisy map  $\mathcal{F}_{T+T'/2}^{2T+T'}$  as

$$\bar{\mathcal{F}}_{T+T'/2}^{2T+T'}(|+\rangle\langle+|^{\otimes N}) = (1-\bar{p})|\phi_{\text{id}}\rangle\langle\phi_{\text{id}}| + \bar{p}\bar{\rho}_e. \quad (\text{D3})$$

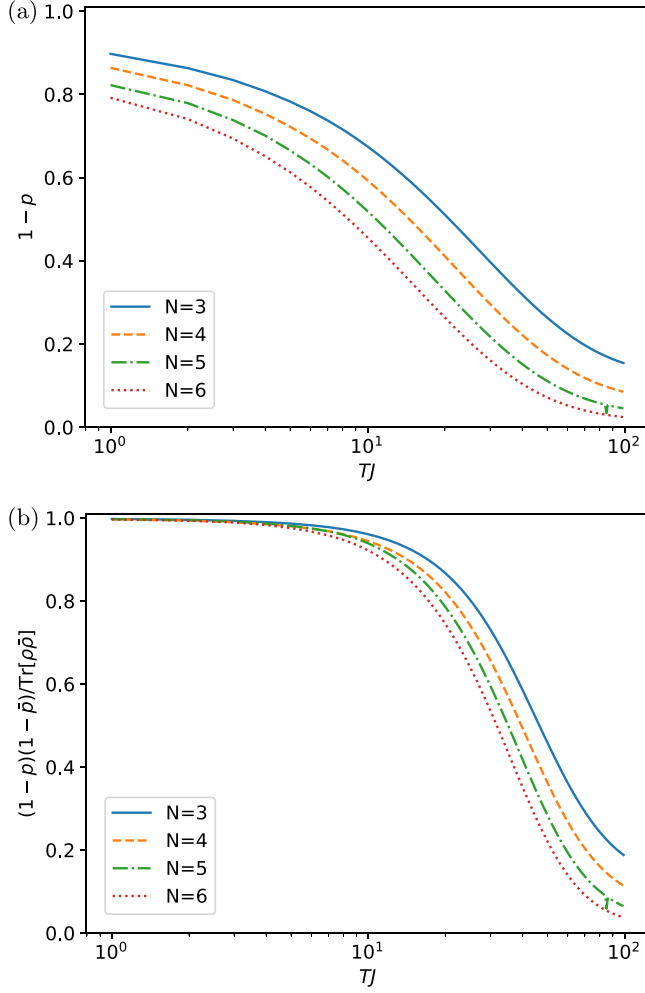


FIG. 9. Populations of the ideal state  $|\phi_{\text{id}}\rangle$  in (a) the density matrix without EM and (b) the virtually purified state (see the main text). All the parameters  $J$ ,  $\Delta$ ,  $B$ ,  $\lambda$ , and  $T'$  and the noise model are the same in the main text. In each case of the number of qubits, the virtually purified state maintains the population close to 1 longer compared to the density matrix without EM.

We can also numerically compute the population of  $|\phi_{\text{id}}\rangle$  in the virtually purified state  $(\rho\bar{\rho} + \bar{\rho}\rho)/2\text{Tr}[\rho\bar{\rho}]$  as follows:

$$\frac{(1-p)(1-\bar{p})}{\text{Tr}[\rho\bar{\rho}]} = \frac{(\tilde{P}^+ - \tilde{P}^-)}{\text{Tr}[\rho\bar{\rho}]}, \quad (\text{D4})$$

where

$$\tilde{P}^\pm = \langle + |^{\otimes N} \mathcal{F}_{T+T'/2}^{2T+T'} [P^\pm \mathcal{F}_0^{T+T'/2} (|+\rangle \langle +|^{\otimes N}) P^\pm] | + \rangle^{\otimes N}, \quad (\text{D5})$$

and  $P^\pm = (I \pm |\phi_{\text{id}}\rangle \langle \phi_{\text{id}}|)/2$ .

We plot the populations  $1-p$  and  $(1-p)(1-\bar{p})/\text{Tr}[\rho\bar{\rho}]$  of  $|\phi_{\text{id}}\rangle$  in Fig. 9. We use the same values for all parameters  $J$ ,  $\Delta$ ,  $B$ ,  $\lambda$ , and  $T'$  and the same noise model as in the main text. The results show that, by using the EMQA schedule, the population of the ideal state is almost the unity for  $TJ \leq 10^{-1}$ . On the other hand, the population of the ideal state during QA without EM is much smaller than that with EM for all  $T$ . This means that we can take a longer annealing time to suppress

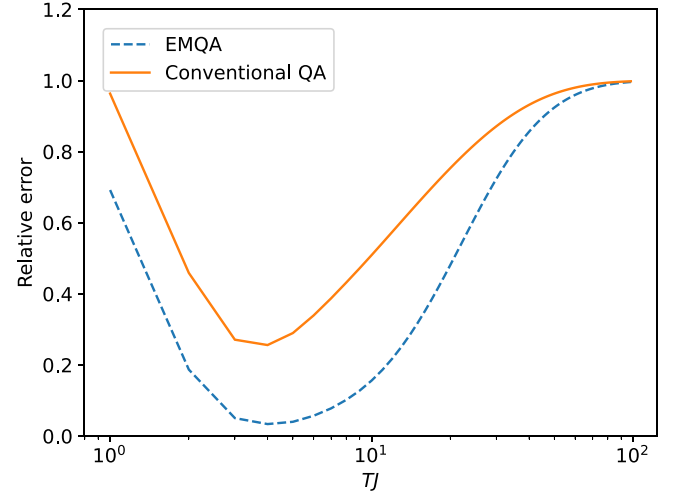


FIG. 10. Relative error of the ground-state energy of the problem Hamiltonian  $H_p$  with the noise model described by the quantum adiabatic master equation. The relative error is defined as  $(\langle H_p \rangle - E_g)/|E_g|$ , which is the same as that in Fig. 4. We adopt (a) the EMQA and (b) the conventional schedule with  $\lambda/J = 0.004$ . We obtain the minimum relative error 0.0338 (0.256) in  $T = 6.37(6.37)$  ns with the EMQA (conventional) method.

the nonadiabatic conditions when we use the EM. Therefore, the numerical results here are consistent with those in Fig. 4, which shows the advantage of the EMQA.

## APPENDIX E: MORE REALISTIC SIMULATION

Here, we investigate the performance of our method when we adopt a more realistic noise model. More specifically, we consider the quantum adiabatic Markovian master equation [131–135]. Let us define the total Hamiltonian for the system and the environment as

$$H_{\text{total}}(t) = H_{\text{sys}}(t) + H_{\text{bath}} + H_{\text{int}}, \quad (\text{E1})$$

where  $H_{\text{sys}}(t)$ ,  $H_{\text{bath}}$ , and  $H_{\text{int}}$  are the system, bath, and interaction Hamiltonian, respectively. In the numerical simulation, we set either  $H_{\text{sys}}(t) = H_{\text{CQA}}(t)$  or  $H_{\text{sys}}(t) = H_{\text{EMQA}}(t)$ . Also, we define the interaction Hamiltonian as  $H_{\text{int}} = \sum_{k=1}^M A_k \otimes B_k$  where  $A_k$  ( $B_k$ ) denotes an operator acting on the system (the bath). We can describe the dynamics of the total Hamiltonian with the von Neumann equation as

$$\frac{d\rho_{\text{total}}}{dt} = -i[H(t), \rho_{\text{total}}]. \quad (\text{E2})$$

By assuming the Born-Markov approximation and small nonadiabatic transitions, we obtain the quantum adiabatic Markovian master equation for the system density matrix  $\rho$  in the interaction picture [133,136,137] as

$$\begin{aligned} \frac{d\rho}{dt} = & \frac{1}{2} \sum_{k,l} \sum_{\omega,\omega'} e^{i(\omega-\omega')t} \Gamma_{kl}(\omega') \\ & \times \{A_l(\omega')\rho A_k^\dagger(\omega) - A_k^\dagger(\omega)A_l(\omega')\rho\} + \text{H.c.}, \quad (\text{E3}) \end{aligned}$$

where  $A_k(\omega) = \sum_{\epsilon' = -\epsilon = \omega} |\psi_{\epsilon'}\rangle\langle\psi_{\epsilon}| A_k |\psi_{\epsilon'}\rangle\langle\psi_{\epsilon}|$  denotes a noise operator associated with the energy  $\omega$ ,  $|\psi_{\epsilon}\rangle$  denotes the instantaneous eigenvector of the Hamiltonian  $H_{\text{sys}}(t)$  with an eigenvalue of  $\epsilon$ , and  $\Gamma_{kl}$  denotes the power spectrum density. Here, we ignore the cross correlations between different indices  $k$  and  $l$  [i.e.,  $\Gamma_{kl}(\omega) = \Gamma(\omega)\delta_{kl}$ ]. We choose the noise operator as  $A_k = \hat{\sigma}_k^z$ . Also, we choose the power spectrum density as

$$\Gamma(\omega) = \begin{cases} \eta\omega\left(\frac{1}{e^{\omega/T_{\text{env}}}-1} + 1\right) & (\omega > 0), \\ \eta T_{\text{env}} & (\omega = 0), \\ \eta(-\omega)\left(\frac{1}{e^{-\omega/T_{\text{env}}}-1} + 1\right) & (\omega < 0), \end{cases} \quad (\text{E4})$$

where  $\eta$  denotes the strength of the decoherence and  $T_{\text{env}}$  denotes the temperature of the environment. For the numerical simulation, we need to set the cutoff parameters  $\omega_c$  and  $\delta$ . Thus, we modify the power spectrum density

as

$$\Gamma(\omega)^{(\text{co})} = \begin{cases} \eta\omega e^{-\omega/\omega_c} \left( \frac{1}{e^{\omega/T_{\text{env}}}-1} + 1 \right) & (\omega > 0), \\ \eta T_{\text{env}} & (\omega = 0), \\ \eta(-\omega) e^{\omega/\omega_c} \left( \frac{1}{e^{-\omega/T_{\text{env}}}-1} + 1 \right) & (\omega < 0). \end{cases} \quad (\text{E5})$$

We set  $\omega_c/J = 20$ ,  $\delta = 10^{-7}$ ,  $\eta = 0.01$ ,  $N = 3$ , and  $T_{\text{env}}/J = 10$  in the numerical simulation. Particularly,  $T_{\text{env}} = 10J\hbar/k_B \simeq 4.8$  mK. This temperature can be achieved in actual devices [138,139].

We plot the relative error of the EMQA and the conventional QA under the effect of decoherence described by the quantum Markovian master equation in Fig. 10. We show that our method provides a more accurate expectation value of the ground-state energy than the conventional method. Therefore, our method is still promising even when we adopt a realistic noise model.

- 
- [1] T. Kadowaki and H. Nishimori, Quantum annealing in the transverse Ising model, *Phys. Rev. E* **58**, 5355 (1998).
  - [2] E. Farhi, J. Goldstone, S. Gutmann, and M. Sipser, Quantum computation by adiabatic evolution, [arXiv:quant-ph/0001106](https://arxiv.org/abs/quant-ph/0001106).
  - [3] E. Farhi, J. Goldstone, S. Gutmann, J. Lapan, A. Lundgren, and D. Preda, A quantum adiabatic evolution algorithm applied to random instances of an NP-complete problem, *Science* **292**, 472 (2001).
  - [4] P. Ray, B. K. Chakrabarti, and A. Chakrabarti, Sherrington-kirkpatrick model in a transverse field: Absence of replica symmetry breaking due to quantum fluctuations, *Phys. Rev. B* **39**, 11828 (1989).
  - [5] A. B. Finnila, M. A. Gomez, C. Sebenik, C. Stenson, and J. D. Doll, Quantum annealing: A new method for minimizing multidimensional functions, *Chem. Phys. Lett.* **219**, 343 (1994).
  - [6] P. Ehrenfest, *Adiabatische Invarianten und Quantentheorie*, *Annal. Physik* **356** (1916).
  - [7] T. Kato, On the adiabatic theorem of quantum mechanics, *J. Phys. Soc. Jpn.* **5**, 435 (1950).
  - [8] M. H. S. Amin, Consistency of the adiabatic theorem, *Phys. Rev. Lett.* **102**, 220401 (2009).
  - [9] A. Dodin and P. Brumer, Generalized adiabatic theorems: Quantum systems driven by modulated time-varying fields, *PRX Quantum* **2**, 030302 (2021).
  - [10] S. Jansen, M.-B. Ruskai, and R. Seiler, Bounds for the adiabatic approximation with applications to quantum computation, *J. Math. Phys.* **48**, 102111 (2007).
  - [11] W. Lechner, P. Hauke, and P. Zoller, A quantum annealing architecture with all-to-all connectivity from local interactions, *Sci. Adv.* **1**, e1500838 (2015).
  - [12] V. Kumar, G. Bass, C. Tomlin, and J. Dulny, Quantum annealing for combinatorial clustering, *Quantum Inf. Proc.* **17**, 1 (2018).
  - [13] V. Choi, Minor-embedding in adiabatic quantum computation: II. minor-universal graph design, *Quantum Inf. Proc.* **10**, 343 (2011).
  - [14] S. Boixo, T. F. Rønnow, S. V. Isakov, Z. Wang, D. Wecker, D. A. Lidar, J. M. Martinis, and M. Troyer, Evidence for quantum annealing with more than one hundred qubits, *Nat. Phys.* **10**, 218 (2014).
  - [15] R. Cleve, A. Ekert, C. Macchiavello, and M. Mosca, Quantum algorithms revisited, *Proc. R. Soc. London, Ser. A* **454**, 339 (1998).
  - [16] B. L. Higgins, D. W. Berry, S. D. Bartlett, M. W. Mitchell, H. M. Wiseman, and G. J. Pryde, Demonstrating Heisenberg-limited unambiguous phase estimation without adaptive measurements, *New J. Phys.* **11**, 073023 (2009).
  - [17] W. van Dam, G. M. D'Ariano, A. Ekert, C. Macchiavello, and M. Mosca, Optimal quantum circuits for general phase estimation, *Phys. Rev. Lett.* **98**, 090501 (2007).
  - [18] P. Hauke, H. G. Katzgraber, W. Lechner, H. Nishimori, and W. D. Oliver, Perspectives of quantum annealing: Methods and implementations, *Rep. Prog. Phys.* **83**, 054401 (2020).
  - [19] V. Kremenetski, C. Mejuto-Zaera, S. J. Cotton, and N. M. Tubman, Simulation of adiabatic quantum computing for molecular ground states, *J. Chem. Phys.* **155**, 234106 (2021).
  - [20] S. Morita and H. Nishimori, Mathematical foundation of quantum annealing, *J. Math. Phys.* **49**, 125210 (2008).
  - [21] M. Albert, *Quantum Mechanics*, Volume I (Wiley, New York, 1961).
  - [22] M. Albert, *Quantum Mechanics*, Volume II (North-Holland, Amsterdam, 1962).
  - [23] J. Roland and N. J. Cerf, Noise resistance of adiabatic quantum computation using random matrix theory, *Phys. Rev. A* **71**, 032330 (2005).
  - [24] J. Åberg, D. Kult, and E. Sjöqvist, Quantum adiabatic search with decoherence in the instantaneous energy eigenbasis, *Phys. Rev. A* **72**, 042317 (2005).
  - [25] T. Albash and D. A. Lidar, Decoherence in adiabatic quantum computation, *Phys. Rev. A* **91**, 062320 (2015).
  - [26] A. M. Childs, E. Farhi, and J. Preskill, Robustness of adiabatic quantum computation, *Phys. Rev. A* **65**, 012322 (2001).
  - [27] M. S. Sarandy and D. A. Lidar, Adiabatic quantum computation in open systems, *Phys. Rev. Lett.* **95**, 250503 (2005).

- [28] S. Ashhab, J. R. Johansson, and F. Nori, Decoherence in a scalable adiabatic quantum computer, *Phys. Rev. A* **74**, 052330 (2006).
- [29] J. Preskill, Quantum computing in the NISQ era and beyond, *Quantum* **2**, 79 (2018).
- [30] S. Endo, Z. Cai, S. C. Benjamin, and X. Yuan, Hybrid quantum-classical algorithms and quantum error mitigation, *J. Phys. Soc. Jpn.* **90**, 032001 (2021).
- [31] M. Cerezo, A. Arrasmith, R. Babbush, S. C. Benjamin, S. Endo, K. Fujii, Jarrod R McClean, K. Mitarai, X. Yuan, L. Cincio *et al.*, Variational quantum algorithms, *Nat. Rev. Phys.* **3**, 625 (2021).
- [32] R. Barends, J. Kelly, A. Megrant, A. Veitia, D. Sank, E. Jeffrey, T. C. White, J. Mutus, A. G. Fowler, B. Campbell *et al.*, Superconducting quantum circuits at the surface code threshold for fault tolerance, *Nature (London)* **508**, 500 (2014).
- [33] K. R. Brown, A. C. Wilson, Y. Colombe, C. Ospelkaus, A. M. Meier, E. Knill, D. Leibfried, and D. J. Wineland, Single-qubit-gate error below  $10^{-4}$  in a trapped ion, *Phys. Rev. A* **84**, 030303(R) (2011).
- [34] A. Peruzzo, J. McClean, P. Shadbolt, M.-H. Yung, X.-Qi Zhou, P. J. Love, A. Aspuru-Guzik, and J. L. O'Brien, A variational eigenvalue solver on a photonic quantum processor, *Nat. Commun.* **5**, 4213 (2014).
- [35] Y. Li and S. C. Benjamin, Efficient variational quantum simulator incorporating active error minimization, *Phys. Rev. X* **7**, 021050 (2017).
- [36] J. R. McClean, J. Romero, R. Babbush, and A. Aspuru-Guzik, The theory of variational hybrid quantum-classical algorithms, *New J. Phys.* **18**, 023023 (2016).
- [37] X. Yuan, S. Endo, Qi Zhao, Y. Li, and S. C. Benjamin, Theory of variational quantum simulation, *Quantum* **3**, 191 (2019).
- [38] S. Endo, J. Sun, Y. Li, S. C. Benjamin, and X. Yuan, Variational quantum simulation of general processes, *Phys. Rev. Lett.* **125**, 010501 (2020).
- [39] A. Kandala, K. Temme, A. D. Córcoles, A. Mezzacapo, J. M. Chow, and J. M. Gambetta, Error mitigation extends the computational reach of a noisy quantum processor, *Nature (London)* **567**, 491 (2019).
- [40] K. Temme, S. Bravyi, and J. M. Gambetta, Error mitigation for short-depth quantum circuits, *Phys. Rev. Lett.* **119**, 180509 (2017).
- [41] S. Endo, S. C. Benjamin, and Y. Li, Practical quantum error mitigation for near-future applications, *Phys. Rev. X* **8**, 031027 (2018).
- [42] C. Song, J. Cui, H. Wang, J. Hao, H. Feng, and Y. Li, Quantum computation with universal error mitigation on a superconducting quantum processor, *Sci. Adv.* **5**, eaaw5686 (2019).
- [43] S. Zhang, Y. Lu, K. Zhang, W. Chen, Y. Li, J.-N. Zhang, and K. Kim, Error-mitigated quantum gates exceeding physical fidelities in a trapped-ion system, *Nat. Commun.* **11**, 1 (2020).
- [44] S. McArdle, X. Yuan, and S. Benjamin, Error-mitigated digital quantum simulation, *Phys. Rev. Lett.* **122**, 180501 (2019).
- [45] X. Bonnet-Monroig, R. Sagastizabal, M. Singh, and T. E. O'Brien, Low-cost error mitigation by symmetry verification, *Phys. Rev. A* **98**, 062339 (2018).
- [46] J. Sun, X. Yuan, T. Tsunoda, V. Vedral, S. C. Benjamin, and S. Endo, Mitigating realistic noise in practical noisy intermediate-scale quantum devices, *Phys. Rev. Appl.* **15**, 034026 (2021).
- [47] R. LaRose, A. Mari, S. Kaiser, P. J. Karalekas, A. A. Alves, P. Czarnik, M. El Mandouh, M. H. Gordon, Y. Hindy, A. Robertson *et al.*, Mitiq: A software package for error mitigation on noisy quantum computers, *Quantum* **6**, 774 (2022).
- [48] Google AI Quantum, Collaborators, F. Arute, K. Arya, R. Babbush, D. Bacon, J. C. Bardin, R. Barends, S. Boixo, M. Broughton, B. B. Buckley *et al.*, Hartree-fock on a superconducting qubit quantum computer, *Science* **369**, 1084 (2020).
- [49] J. R. McClean, M. E. Kimchi-Schwartz, J. Carter, and W. A. De Jong, Hybrid quantum-classical hierarchy for mitigation of decoherence and determination of excited states, *Phys. Rev. A* **95**, 042308 (2017).
- [50] S. T. Merkel, J. M. Gambetta, J. A. Smolin, S. Poletto, A. D. Córcoles, B. R. Johnson, C. A. Ryan, and M. Steffen, Self-consistent quantum process tomography, *Phys. Rev. A* **87**, 062119 (2013).
- [51] C. Stark, Self-consistent tomography of the state-measurement gram matrix, *Phys. Rev. A* **89**, 052109 (2014).
- [52] D. Greenbaum, Introduction to quantum gate set tomography, [arXiv:1509.02921](https://arxiv.org/abs/1509.02921).
- [53] R. Blume-Kohout, J. K. Gamble, E. Nielsen, K. Rudinger, J. Mizrahi, K. Fortier, and P. Maunz, Demonstration of qubit operations below a rigorous fault tolerance threshold with gate set tomography, *Nat. Commun.* **8**, 14485 (2017).
- [54] A. Strikis, D. Qin, Y. Chen, S. C. Benjamin, and Y. Li, Learning-based quantum error mitigation, *PRX Quantum* **2**, 040330 (2021).
- [55] P. Czarnik, A. Arrasmith, P. J. Coles, and L. Cincio, Error mitigation with clifford quantum-circuit data, *Quantum* **5**, 592 (2021).
- [56] Z. Wang, Y. Chen, Z. Song, D. Qin, H. Li, Q. Guo, H. Wang, C. Song, and Y. Li, Scalable evaluation of quantum-circuit error loss using clifford sampling, *Phys. Rev. Lett.* **126**, 080501 (2021).
- [57] T. E. O'Brien, S. Polla, N. C. Rubin, W. J. Huggins, S. McArdle, S. Boixo, J. R. McClean, and R. Babbush, Error mitigation via verified phase estimation, *PRX Quantum* **2**, 020317 (2021).
- [58] N. Yoshioka, H. Hakoshima, Y. Matsuzaki, Y. Tokunaga, Y. Suzuki, and S. Endo, Generalized quantum subspace expansion, *Phys. Rev. Lett.* **129**, 020502 (2022).
- [59] Z. Cai, R. Babbush, S. C. Benjamin, S. Endo, W. J. Huggins, Y. Li, J. R. McClean, and T. E. O'Brien, Quantum error mitigation, *Rev. Mod. Phys.* **95**, 045005 (2023).
- [60] C. Cao, Y. Yu, Z. Wu, N. Shannon, B. Zeng, and R. Joynt, Mitigating algorithmic errors in quantum optimization through energy extrapolation, *Quantum Sci. Technol.* (to be published).
- [61] M. Huo and Y. Li, Self-consistent tomography of temporally correlated errors, *Commun. Theor. Phys.* **73**, 075101 (2021).
- [62] R. Takagi, Optimal resource cost for error mitigation, *Phys. Rev. Res.* **3**, 033178 (2021).
- [63] H. Hakoshima, Y. Matsuzaki, and S. Endo, Relationship between costs for quantum error mitigation and non-Markovian measures, *Phys. Rev. A* **103**, 012611 (2021).
- [64] Y. Suzuki, S. Endo, K. Fujii, and Y. Tokunaga, Quantum error mitigation as a universal error reduction technique:

- Applications from the NISQ to the fault-tolerant quantum computing eras, *PRX Quantum* **3**, 010345 (2022).
- [65] B. Koczor, Exponential error suppression for near-term quantum devices, *Phys. Rev. X* **11**, 031057 (2021).
- [66] W. J. Huggins, S. McArdle, T. E. O'Brien, J. Lee, N. C. Rubin, S. Boixo, K. B. Whaley, R. Babbush, and J. R. McClean, Virtual distillation for quantum error mitigation, *Phys. Rev. X* **11**, 041036 (2021).
- [67] P. Czarnik, A. Arrasmith, L. Cincio, and P. J. Coles, Qubit-efficient exponential suppression of errors, [arXiv:2102.06056](https://arxiv.org/abs/2102.06056).
- [68] K. Yamamoto, S. Endo, H. Hakoshima, Y. Matsuzaki, and Y. Tokunaga, Error-mitigated quantum metrology via virtual purification, *Phys. Rev. Lett.* **129**, 250503 (2022).
- [69] M. Huo and Y. Li, Dual-state purification for practical quantum error mitigation, *Phys. Rev. A* **105**, 022427 (2022).
- [70] Y. Susa, Yu Yamashiro, M. Yamamoto, and H. Nishimori, Exponential speedup of quantum annealing by inhomogeneous driving of the transverse field, *J. Phys. Soc. Jpn.* **87**, 023002 (2018).
- [71] Y. Susa, Yu Yamashiro, M. Yamamoto, I. Hen, D. A. Lidar, and H. Nishimori, Quantum annealing of the  $p$ -spin model under inhomogeneous transverse field driving, *Phys. Rev. A* **98**, 042326 (2018).
- [72] Y. Seki and H. Nishimori, Quantum annealing with antiferromagnetic fluctuations, *Phys. Rev. E* **85**, 051112 (2012).
- [73] Y. Seki and H. Nishimori, Quantum annealing with antiferromagnetic transverse interactions for the Hopfield model, *J. Phys. A: Math. Theor.* **48**, 335301 (2015).
- [74] Y. Matsuzaki, H. Hakoshima, K. Sugisaki, Y. Seki, and S. Kawabata, Direct estimation of the energy gap between the ground state and excited state with quantum annealing, *Jpn. J. Appl. Phys.* **60**, SBB102 (2021).
- [75] A. E. Russo, K. M. Rudinger, B. C. A. Morrison, and A. D. Baczewski, Evaluating energy differences on a quantum computer with robust phase estimation, *Phys. Rev. Lett.* **126**, 210501 (2021).
- [76] Y. Mori, S. Kawabata, and Y. Matsuzaki, How to evaluate the adiabatic condition for quantum annealing in an experiment, [arXiv:2208.02553](https://arxiv.org/abs/2208.02553).
- [77] K. Kudo, Constrained quantum annealing of graph coloring, *Phys. Rev. A* **98**, 022301 (2018).
- [78] T. Imoto, Y. Seki, and Y. Matsuzaki, Quantum annealing with symmetric subspaces, [arXiv:2209.09575](https://arxiv.org/abs/2209.09575).
- [79] A. del Campo, Shortcuts to adiabaticity by counterdiabatic driving, *Phys. Rev. Lett.* **111**, 100502 (2013).
- [80] D. Sels and A. Polkovnikov, Minimizing irreversible losses in quantum systems by local counterdiabatic driving, *Proc. Natl. Acad. Sci. USA* **114**, E3909 (2017).
- [81] P. W. Claeys, M. Pandey, D. Sels, and A. Polkovnikov, Floquet-engineering counterdiabatic protocols in quantum many-body systems, *Phys. Rev. Lett.* **123**, 090602 (2019).
- [82] G. Passarelli, V. Cataudella, R. Fazio, and P. Lucignano, Counterdiabatic driving in the quantum annealing of the  $p$ -spin model: A variational approach, *Phys. Rev. Res.* **2**, 013283 (2020).
- [83] Z. Sun, L. Zhou, G. Xiao, D. Poletti, and J. Gong, Finite-time Landau-Zener processes and counterdiabatic driving in open systems: Beyond Born, Markov, and rotating-wave approximations, *Phys. Rev. A* **93**, 012121 (2016).
- [84] P. R. Hegde, G. Passarelli, A. Scooco, and P. Lucignano, Genetic optimization of quantum annealing, *Phys. Rev. A* **105**, 012612 (2022).
- [85] Y. Susa and H. Nishimori, Variational optimization of the quantum annealing schedule for the Lechner-Hauke-Zoller scheme, *Phys. Rev. A* **103**, 022619 (2021).
- [86] D. Guéry-Odelin, A. Ruschhaupt, A. Kiely, E. Torrontegui, S. Martínez-Garaot, and J. G. Muga, Shortcuts to adiabaticity: Concepts, methods, and applications, *Rev. Mod. Phys.* **91**, 045001 (2019).
- [87] S. Deffner, C. Jarzynski, and A. del Campo, Classical and quantum shortcuts to adiabaticity for scale-invariant driving, *Phys. Rev. X* **4**, 021013 (2014).
- [88] T. Yan, B.-J. Liu, K. Xu, C. Song, S. Liu, Z. Zhang, H. Deng, Z. Yan, H. Rong, K. Huang, M. H. Yung, Y. Chen, and D. Yu, Experimental realization of nonadiabatic shortcut to non-Abelian geometric gates, *Phys. Rev. Lett.* **122**, 080501 (2019).
- [89] N. N. Hegade, K. Paul, Y. Ding, M. Sanz, F. Albarrán-Arriagada, E. Solano, and Xi. Chen, Shortcuts to adiabaticity in digitized adiabatic quantum computing, *Phys. Rev. Appl.* **15**, 024038 (2021).
- [90] S. Campbell and S. Deffner, Trade-off between speed and cost in shortcuts to adiabaticity, *Phys. Rev. Lett.* **118**, 100601 (2017).
- [91] A. Del Campo and K. Kim, Focus on shortcuts to adiabaticity, *New J. Phys.* **21**, 050201 (2019).
- [92] M. Nakahara, Counterdiabatic formalism of shortcuts to adiabaticity, *Philos. Trans. R. Soc. A* **380**, 20210272 (2022).
- [93] A. Patra and C. Jarzynski, Shortcuts to adiabaticity using flow fields, *New J. Phys.* **19**, 125009 (2017).
- [94] K. Takahashi, Shortcuts to adiabaticity for quantum annealing, *Phys. Rev. A* **95**, 012309 (2017).
- [95] K. L. Pudenz, T. Albash, and D. A. Lidar, Error-corrected quantum annealing with hundreds of qubits, *Nat. Commun.* **5**, 3243 (2014).
- [96] T. Suzuki and H. Nakazato, A proposal of noise suppression for quantum annealing, [arXiv:2006.13440](https://arxiv.org/abs/2006.13440).
- [97] H. Chen, Xi. Kong, Bo. Chong, G. Qin, X. Zhou, X. Peng, and J. Du, Experimental demonstration of a quantum annealing algorithm for the traveling salesman problem in a nuclear-magnetic-resonance quantum simulator, *Phys. Rev. A* **83**, 032314 (2011).
- [98] M. Nakahara, *Lectures on Quantum Computing, Thermodynamics and Statistical Physics*, Volume 8 (World Scientific, Singapore, 2013).
- [99] Y. Matsuzaki, H. Hakoshima, Y. Seki, and S. Kawabata, Quantum annealing with capacitive-shunted flux qubits, *Jpn. J. Appl. Phys.* **59**, SGGI06 (2020).
- [100] E. Crosson, E. Farhi, C. Yen-Yu Lin, H.-H. Lin, and P. Shor, Different strategies for optimization using the quantum adiabatic algorithm, [arXiv:1401.7320](https://arxiv.org/abs/1401.7320).
- [101] H. Goto and T. Kanao, Quantum annealing using vacuum states as effective excited states of driven systems, *Commun. Phys.* **3**, 235 (2020).
- [102] L. Hormozi, E. W. Brown, G. Carleo, and M. Troyer, Nonstoquastic Hamiltonians and quantum annealing of an Ising spin glass, *Phys. Rev. B* **95**, 184416 (2017).
- [103] S. Muthukrishnan, T. Albash, and D. A. Lidar, Tunneling and speedup in quantum optimization for permutation-symmetric problems, *Phys. Rev. X* **6**, 031010 (2016).

- [104] L. T. Brady and W. van Dam, Necessary adiabatic run times in quantum optimization, *Phys. Rev. A* **95**, 032335 (2017).
- [105] R. D. Somma, D. Nagaj, and M. Kieferová, Quantum speedup by quantum annealing, *Phys. Rev. Lett.* **109**, 050501 (2012).
- [106] A. Das and B. K. Chakrabarti, Colloquium: Quantum annealing and analog quantum computation, *Rev. Mod. Phys.* **80**, 1061 (2008).
- [107] V. Karanikolas and S. Kawabata, Pulsed quantum annealing, *J. Phys. Soc. Jpn.* **89**, 094003 (2020).
- [108] S. Watabe, Y. Seki, and S. Kawabata, Enhancing quantum annealing performance by a degenerate two-level system, *Sci. Rep.* **10**, 1 (2020).
- [109] S. Matsuura, S. Buck, V. Senicourt, and A. Zaribafiyani, Variationally scheduled quantum simulation, *Phys. Rev. A* **103**, 052435 (2021).
- [110] G. Passarelli, R. Fazio, and P. Lucignano, Optimal quantum annealing: A variational shortcut-to-adiabaticity approach, *Phys. Rev. A* **105**, 022618 (2022).
- [111] T. Imoto, Y. Seki, Y. Matsuzaki, and S. Kawabata, Quantum annealing with twisted fields, *New J. Phys.* **24**, 113009 (2022).
- [112] B. Koczor, The dominant eigenvector of a noisy quantum state, *New J. Phys.* **23**, 123047 (2021).
- [113] G. Lindblad, On the generators of quantum dynamical semigroups, *Commun. Math. Phys.* **48**, 119 (1976).
- [114] V. Gorini, A. Kossakowski, and E. Chandy George Sudarshan, Completely positive dynamical semigroups of  $n$ -level systems, *J. Math. Phys.* **17**, 821 (1976).
- [115] Adrian Parra-Rodríguez, P. Lougovski, L. Lamata, E. Solano, and M. Sanz, Digital-analog quantum computation, *Phys. Rev. A* **101**, 022305 (2020).
- [116] J. H. Plantenberg, P. C. De Groot, C. J. P. M. Harmans, and J. E. Mooij, Demonstration of controlled-not quantum gates on a pair of superconducting quantum bits, *Nature (London)* **447**, 836 (2007).
- [117] T. Imoto, Y. Seki, Y. Matsuzaki, and S. Kawabata, Guaranteed-accuracy quantum annealing, *Phys. Rev. A* **106**, 042615 (2022).
- [118] T. Imoto, Y. Seki, and Y. Matsuzaki, Obtaining ground states of the XXZ model using the quantum annealing with inductively coupled superconducting flux qubits, *J. Phys. Soc. Jpn.* **91**, 064004 (2022).
- [119] F. Yan, S. Gustavsson, A. Kamal, J. Birenbaum, A. P. Sears, D. Hover, T. J. Gudmundsen, D. Rosenberg, G. Samach, S. Weber *et al.*, The flux qubit revisited to enhance coherence and reproducibility, *Nat. Commun.* **7**, 12964 (2016).
- [120] R. Harris, T. Lanting, A. J. Berkley, J. Johansson, M. W. Johnson, P. Bunyk, E. Ladizinsky, N. Ladizinsky, T. Oh, and S. Han, Compound Josephson-junction coupler for flux qubits with minimal crosstalk, *Phys. Rev. B* **80**, 052506 (2009).
- [121] F. Yan, P. Krantz, Y. Sung, M. Kjaergaard, D. L. Campbell, T. P. Orlando, S. Gustavsson, and W. D. Oliver, Tunable coupling scheme for implementing high-fidelity two-qubit gates, *Phys. Rev. Appl.* **10**, 054062 (2018).
- [122] X. Li, T. Cai, H. Yan, Z. Wang, X. Pan, Y. Ma, W. Cai, J. Han, Z. Hua, X. Han *et al.*, Tunable coupler for realizing a controlled-phase gate with dynamically decoupled regime in a superconducting circuit, *Phys. Rev. Appl.* **14**, 024070 (2020).
- [123] J. J. Wallman and J. Emerson, Noise tailoring for scalable quantum computation via randomized compiling, *Phys. Rev. A* **94**, 052325 (2016).
- [124] J Robert Johansson, P. D. Nation, and F. Nori, Qutip: An open-source python framework for the dynamics of open quantum systems, *Comput. Phys. Commun.* **183**, 1760 (2012).
- [125] A. Perdomo-Ortiz, S. E. Venegas-Andraca, and A. Aspuru-Guzik, A study of heuristic guesses for adiabatic quantum computation, *Quantum Inf. Proc.* **10**, 33 (2011).
- [126] M. Ohkuwa, H. Nishimori, and D. A. Lidar, Reverse annealing for the fully connected  $p$ -spin model, *Phys. Rev. A* **98**, 022314 (2018).
- [127] G. Passarelli, Ka-Wa Yip, D. A. Lidar, H. Nishimori, and P. Lucignano, Reverse quantum annealing of the  $p$ -spin model with relaxation, *Phys. Rev. A* **101**, 022331 (2020).
- [128] D. Venturelli and A. Kondratyev, Reverse quantum annealing approach to portfolio optimization problems, *Quantum Mach. Intell.* **1**, 17 (2019).
- [129] J. King, M. Mohseni, W. Bernoudy, Alexandre Fréchette, H. Sadeghi, S. V. Isakov, H. Neven, and M. H. Amin, Quantum-assisted genetic algorithm, [arXiv:1907.00707](https://arxiv.org/abs/1907.00707).
- [130] Yu Yamashiro, M. Ohkuwa, H. Nishimori, and D. A. Lidar, Dynamics of reverse annealing for the fully connected  $p$ -spin model, *Phys. Rev. A* **100**, 052321 (2019).
- [131] A. G. Redfield, On the theory of relaxation processes, *IBM J. Res. Dev.* **1**, 19 (1957).
- [132] A. G. Redfield, in *Advances in Magnetic Resonance*, volume 1 of *Advances in Magnetic and Optical Resonance*, edited by J. S. Waugh (Academic Press, New York, 1965), pp. 1–32.
- [133] T. Albash, S. Boixo, D. A. Lidar, and P. Zanardi, Quantum adiabatic Markovian master equations, *New J. Phys.* **14**, 123016 (2012).
- [134] A. Rivas and S. F. Huelga, *Open Quantum Systems*, Volume 10 (Springer, Berlin, 2012).
- [135] Heinz-Peter Breuer, F. Petruccione *et al.*, *The Theory of Open Quantum Systems* (Oxford University Press, Oxford, 2002).
- [136] T. Imoto and Y. Matsuzaki, Catastrophic failure of quantum annealing owing to non-stoquastic Hamiltonian and its avoidance by decoherence, [arXiv:2209.10983](https://arxiv.org/abs/2209.10983).
- [137] K. Hornberger, Introduction to decoherence theory, in *Entanglement and Decoherence: Foundations and Modern Trends* (Springer, Berlin, 2009), pp. 221–276.
- [138] G. C. Knee, K. Kakuyanagi, M.-C. Yeh, Y. Matsuzaki, H. Toida, H. Yamaguchi, S. Saito, A. J. Leggett, and W. J. Munro, A strict experimental test of macroscopic realism in a superconducting flux qubit, *Nat. Commun.* **7**, 13253 (2016).
- [139] M. Kounalakis, G. E. W. Bauer, and Y. M. Blanter, Analog quantum control of magnonic cat states on a chip by a superconducting qubit, *Phys. Rev. Lett.* **129**, 037205 (2022).